843

TECHNICAL MEMORANDUM

Assimilation of SMOS brightness temperatures in the ECMWF Integrated Forecasting System

J. Muñoz-Sabater[1], H. Lawrence[1], C. Albergel[2], P. de Rosnay[1], L. Isaksen[1], S. Mecklenburg[3], Y. Kerr[4], M. Drusch[5]

Research Department

[1] ECMWF, Reading, UK, [2] CNRM, Toulouse, France, [3] ESA-ESRIN, Frascati, Italy, [4] CESBIO, Toulouse, France, [5] ESA-ESTEC, Noordwijk, The Netherlands

European Centre for Medium-Range Weather Forecasts
Europäisches Zentrum für mittelfristige Wettervorhersage
Centre européen pour les prévisions météorologiques à moyen terme

Series: ECMWF Technical Memoranda

A full list of ECMWF Publications can be found on our web site under:
http://www.ecmwf.int/en/research/publications

Contact: library@ecmwf.int

Abstract

The assimilation of SMOS brightness temperatures (T_B) data in Numerical Weather Prediction Systems influences the state of the soil, which in turn affects the exchange of energy and water fluxes between the soil and the near surface atmosphere, with potential implications in the prediction of atmospheric variables. In this paper, the impact of assimilating SMOS T_B alone or in combination with screen level observations and ASCAT soil moisture retrievals, on land surface and near-surface atmospheric variables, is assessed. Independent quality controlled in situ soil moisture observations belonging to several networks included in the International Soil Moisture Network were used to validate the quality of both the new soil moisture analyses and the skill to predict soil moisture up to 5 days ahead. The impact on atmospheric variables is indirect and it was evaluated through computation of the forecast skill at different lead times. The analysis period was selected around the boreal summer, a period of the year when evaporatranspiration fluxes are stronger, and when it is therefore expected that the assimilation of remote sensing data provides the largest impact on the state of the soil. The results show that the soil moisture state benefits from the direct assimilation of SMOS T_B, especially in better representing the temporal variations of soil moisture in time. The skill on atmospheric variables is mainly driven by the screen level observations. Despite the clear benefits on the soil state, remote sensing data needs to be used with screen level variables to add value on the state of the atmosphere, pointing to inconsistencies in the physical coupling between the land and near-surface components of the ECMWF Earth system.

1   Introduction

An accurate description of the current state of the land surface is essential for numerical weather prediction (NWP), as it determines the lower boundary conditions for the atmospheric processes. Over snow-free and unfrozen soils, root-zone soil moisture is the soil variable of particular interest as it has a strong influence on the exchange of energy and water fluxes between the land and the atmosphere. A significant number of studies in the literature have shown the impact of initial soil moisture conditions on short and medium-range weather forecasts (e.g. [Beljaars et al., 1996, Mahfouf et al., 2000, Douville et al., 2000, Drusch and Viterbo, 2007, Van-Den-Hurk et al., 2008]) and even at longer time scales covering seasons ([Koster et al., 2010, Koster et al., 2011, Weisheimer et al., 2011, Materia et al., 2014, Prodhomme et al., 2016]). Consequently, a lot of resources have been devoted to integrate novel satellite measurements related to soil moisture in NWP, improving data assimilation schemes and quantifying the impact on the forecast skill.

Already in 1995 [Viterbo and Beljaars, 1995] pointed out that excessive solar radiation at the surface in the European Centre for Medium-Range Weather Forecasts (ECMWF) scheme, due for example to a deficiency in the model clouds, led to an excessive drying of the surface, and thus too little precipitation and cloud cover formation. A nudging scheme was implemented ([Viterbo, 1996]), where the soil moisture increments were computed from the specific humidity increments at the lowest model level using a single empirical regression coefficient. While this scheme prevented the free running soil moisture from drifting, the resulting soil moisture was unrealistic, the main reason being that the nudging scheme compensated for model biases and did so too rapidly. This shortcoming motivated the implementation of an Optimal Interpolation (OI) scheme that assimilated simultaneously near surface temperature and humidity observations, as proposed by [Mahfouf, 1991] and evaluated by [Douville et al., 2000]. Screen level variable assimilation benefits from the availability of large number of consolidated ground stations providing reliable 2 meter temperature and relative humidity measurements. However, the density of these stations is not homogeneous around the world, being much denser in developed countries whereas in vast areas of Africa and Asia only a few stations exist. But the main disadvantage of this assimilation approach

is that screen level observations are not always directly linked with the underlying soil under certain weather conditions. For instance, screen level variables and soil moisture can be decoupled in synoptic situations characterized by weak radiative forcing, strong precipitation, or high wind speeds. The assimilation of screen level parameters resulted in improved atmospheric forecasts while at the same time the accuracy of the soil moisture analyses was degraded ([Drusch and Viterbo, 2007]). In this scheme, soil moisture is used as a sink term, where errors accumulate, in order to satisfy land-atmosphere fluxes exchange. The development and implementation at ECMWF of a point-scale Simplified Extended Kalman Filter (SEKF) ([Seuffert et al., 2004, Drusch et al., 2009b, de Rosnay et al., 2013]) provided more coherence to soil moisture analyses, especially at the root-zone level, and made the system more flexible to accomodate the increasing number of satellite data sensitive to soil moisture. The implementation of the SEKF permitted the operational assimilation of ASCAT soil moisture retrievals since summer 2015 at ECMWF.

Since the early 90s low frequency microwave remote sensing has offered the opportunity to derive more direct estimates of soil moisture with the required temporal and spatial resolution and sampling. The first global data sets providing reliable soil moisture estimates on a routine basis have been derived from the C-band scatterometers onboard ERS-1/2 ([Wagner et al., 1999]) and METOP-A,B ([Bartalis et al., 2007, Wagner et al., 2007, Albergel et al., 2009, Wagner et al., 2013]. Since 2002, the Advanced Microwave Scanning Radiometer (AMSR) series offers low frequency passive microwave observations that have been used for soil moisture retrievals, yielding an absolute accuracy of approximately 6% volumetric soil moisture. These active and passive observations have been complemented with measurements from various systems, such as TMI onboard TRMM ([Gao et al., 2006]), Windsat ([Li et al., 2010]), SSMI ([Wen et al., 2005]), ASCAT ([Wagner et al., 2013]) and Sentinel-1 ([Gao et al., 2017]). In parallel to these developments of the observation capabilities, [Reichle and Koster, 2005] pioneered the assimilation of microwave measurements into land surface models demonstrating the positive impact on the soil moisture analysis.

Yet, none of the satellite instruments above had as prime objective providing information on soil moisture. SMOS, the first satellite specifically designed to infer soil moisture and ocean salinity, was launched in 2009 ([Kerr et al., 2010, Kerr et al., 2012, Mecklenburg et al., 2016]). SMOS is operating at L-band (1.4. GHz) where the sensitivity to surface properties is high due to an increased penetration depth and a reduced sensitivity to vegetation properties when compared to measurements taken at higher frequencies. The SMOS payload data ground segments generates brightness temperature (T$_B$) data over land with an Near Real Time (NRT) product latency of less than 3 hours for NWP applications and other time critical applications such as flood forecasting. The soil moisture products originating from SMOS are generally of high-quality ([Kerr et al., 2012, Kerr et al., 2016]) meeting the targeted accuracy of 4% volumetric soil moisture and a number of studies indicate a positive analysis impact when the observations were assimilated in their systems (e.g. [Lievens et al., 2015, de Lannoy and Reichle, 2016b, Lievens et al., 2016]). However, integrating coarse resolution satellite observations from low frequency microwave measurements (which represent the top 1 to 5 centimeters of the soil) into land surface models, remains a challenge with respect to, among others, observation operators, bias correction schemes (e.g. [Drusch et al., 2005, Verhoest et al., 2015]), and the characterization of model and observation errors.

At ECMWF, the preparations for integrating SMOS observations started in 2001 with first feasibility studies using the SEKF ([Seuffert et al., 2004]). Since then ECMWF has developed both, the capability to acquire, ingest, pre-process and monitor SMOS NRT T$_B$ ([Muñoz-Sabater et al., 2012]) and to assimilate SMOS data integrated as another component of the ECMWF Land Data Assimilation System ([Muñoz-Sabater, 2015]). The ECMWF root-zone soil moisture retrieval algorithm used in this study optimally combines SMOS Level-1 NRT T$_B$ observations with ECMWF forward modeled T$_B$ into the SEKF data assimilation system. A number of analyses have been performed to optimize the parameters in

the microwave emission model used as the forward operator generating T_B at the top of the atmosphere. In addition, a bias correction scheme using the Cumulative Density Function (CDF) matching approach was implemented to reduce systematic differences between the model background and the measurements ([de Rosnay et al., 2018]). Apart from these developments, several technical challenges addressing the large data volume and the increased computational time required for the new surface analysis using satellite observations needed to be solved.

In this paper we analyze how the water content in the top one meter of the soil and lower troposphere numerical weather predictions benefit from the combined assimilation of screen level variables and remotely sensed observations. We perform several long experiments assimilating SMOS T_B, alone or in combination with screen level variables and ASCAT soil moisture retrievals. Following this introduction, section 2 provides a description of the data used in this study, as well as the methodology and the experimental set up conducted in this paper. The experimental results are presented in section 3. Some important aspects of this study are discussed in section 4, and finally the conclusions of this study are collected and presented in section 5.

2 Material and Methods

2.1 Assimilated Observations

2.1.1 Conventional land observations

In situ observations of air temperature and relative humidity at the screen level (two meter above the land surface) are routinely available in NRT from the SYNOP network. In the past two decades, several operational centers have used these observations (referred to hereafter as Screen Level Variables (SLV)) to analyze soil moisture for operational NWP applications ([Mahfouf et al., 2000, de Rosnay et al., 2013]). In the current ECMWF system, more than 35,000 SYNOP SLV observations, covering continental areas across the world, are assimilated daily in the land data assimilation system. Prior to their use in the soil moisture analysis, SLV observations are analyzed and regridded over all land grid points using a two-dimensional Optimal Interpolation (2D-OI) scheme. The maximum number of observations allowed to influence the analysis value at a model grid point is 50, with a search radius around the grid-point location of 1000 km. The influence of the SYNOP observations on a given model grid-point decreases proportionally to the distance from the grid point (see more information in [IFS documentation, 2017]). The outcome of this process is a series of 2 m temperature and 2 m relative humidity pseudo-observations used for the adjustment of soil moisture. The use of these pseudo-observations to analyze soil moisture relies on the coupling processes between soil moisture and near surface atmospheric temperature and humidity conditions. In other words, 2 m air temperature and relative humidity errors in the model background are assumed to be related to corresponding errors in the model soil moisture.

2.1.2 ASCAT soil moisture retrievals

ASCAT is a C-band (5.255 GHz) real aperture radar on board the EUMETSAT (European Organisation for the Exploitation of Meteorological Satellites) MetOp-A and MetOp-B operational meteorological satellites that were launched in 2006 and 2012, respectively. MetOp-C was launched on 7 November 2018, and it carries a third ASCAT instrument. Initially designed for ocean wind speed and direction monitoring, ASCAT is also used to retrieve sea ice properties in polar areas and surface soil moisture over land surfaces ([Wagner et al., 2013]). The ASCAT nominal resolution is 30-50 km, and the ASCAT level

2 gridded soil moisture products are available at 12.5 km and 25 km resolutions, with a 82% daily global coverage for each MetOp satellite. The ASCAT soil moisture product retrieval algorithm was developed by the University of Vienna (TU-Wien) as described by [Bartalis et al., 2007] and [Wagner et al., 2013], and is based on a change detection approach. Seasonal vegetation effects are corrected by accounting for the yearly cycle of the backscatter(σ^0)-incidence angle(θ) relationship. This relationship is important because soil moisture information is gained from the slope and temporal variation of θ and σ^0 (see for ex. [Naeimi et al., 2009]). The resulting ASCAT soil moisture is expressed in terms of soil water index and it is representative of the top 2 cm of the soil. At ECMWF, the soil moisture analysis assimilates the ASCAT Level-2 25 km soil moisture product, and this is the ASCAT product assimilated in this study. The quality control discards data with noise level larger than 8 as well as observations contaminated by the presence of water bodies (water fraction larger than 15%), or topographic complexity larger than 20% ([Scipal et al., 2005]).

2.1.3   SMOS T_B

Launched in November 2009 as one of ESA's Earth Explorer missions, SMOS carries a novel interferometric radiometer operating in the L-band at 1.4 GHz ([Kerr et al., 2010]). The spatial resolution of SMOS raw observations ranges from 35 to 50 km depending on the incidence angle and the geographical location of the observation. The product received and used at ECMWF is the NRT T_B product, which is processed onto a fixed hexagonal grid with approximately 15 km node separation.

Prior to assimilation in the ECMWF Integrated Forecasting System (IFS), all observations are subjected to basic quality checks, followed by a data thinning filter that is necessary due to the vast amount of data available (see [Muñoz-Sabater et al., 2012]). The ECMWF spectral TL511 reduced Gaussian grid (approximately equivalent to 40 km horizontal grid) was selected for the analysis and the NRT T_B data converted to this grid. The latter matches better the original resolution of the SMOS observations and avoids horizontal correlations present in the oversampled NRT product, which are difficult to handle in a data assimilation system. This upscaling step is equivalent to converting the original NRT product to the NRT light BUFR product (see https://earth.esa.int/web/guest/data-access/browse-data-products/-/article/nrt-bufr-light-smos-miras-nrt_bufr_light). It also acts as a data thinning step, frequently used with most satellite sensors delivering radiances at ECMWF. Only three incidence angles were selected and assimilated: 30°, 40° and 50°, as for these angles monthly linear rescaling coefficients where computed (see section 2.2). The margin around each incidence angle was set to ±1°, i.e., observations in the bins [29-31], [39-41] and [49-51] were only considered. For each node of the model grid and angular bin, the observations were averaged with the objective of reducing angular noise, following [Muñoz-Sabater et al., 2014b]. Only the pure X and Y polarisations (X and Y are the H and V polarisations in the antenna frame, and thus different from those at ground level) were used and assimilated in the antenna reference frame, for which the model equivalents were rotated to be in the same reference as the observations. Although the antenna views a large area of several thousands of km, due instrument design, the useful field of view is limited by aliases. Some can be corrected but the signal is pure in a limited hexagon-like shape; the so-called the alias-free zone. This is the zone without ambiguity in the phase-difference and therefore the area of higher quality. Therefore, only observations located in the alias-free field of view were considered. SMOS observations are affected by Radio Frequency Interference (RFI) ([Daganzo-Eusebio et al., 2013, Oliva et al., 2016]). In this paper the RFI flag contained in the BUFR product was used to discard nodes affected by a high probability of RFI contamination. This filtering method based on flags does not guarantee observations free of RFI, but at least some of the most contaminant sources will be filtered out. Finally, prior to use in the assimilation scheme, only observations unaffected by snow or freezing soils (according to 2 m tem-
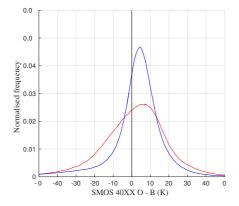
perature and the snow depth short range 12h forecast), as well as by water surfaces and high orography, were selected.

2.2 Rescaling of remote sensing data

Data assimilation methods assume that the observations assimilated are unbiased. Therefore it is crucial to minimize systematic differences with the corresponding model-based estimates. The approach used in this study for both SMOS T$_B$ and ASCAT soil moisture retrievals is a point-wise CDF matching following the approach in [Reichle and Koster, 2004, Scipal et al., 2008, Draper et al., 2012]. The observations monthly mean and standard deviation were linearly rescaled to match the climatologies of the model counterparts, which in this case was the model simulating T$_B$ at the top of the atmosphere and the soil moisture first-guess estimated by the land surface model. For SMOS, the CDF matching technique was applied using SMOS data corresponding to four years of reprocessed data, from 2010 to 2013. Two monthly linear correction coefficients (one correcting for the mean value and another one for the standard deviation) were obtained individually for each month and used to eliminate systematic biases between observations and model equivalents (see [de Rosnay et al., 2018]). The monthly coefficients intend to account for the seasonality of biases in T$_B$.

Fig. 1 shows the histogram of the innovation vector (SMOS T$_B$ minus model equivalent) at 40° incidence angle before (red curve) and after (blue curve) T$_B$ bias correction using the CDF matching technique. Left panel is for the X polarization and right panel for the Y polarization. The shape of the distribution becomes more Gaussian after bias correction, especially for the X polarization, with a larger number of innovations close to zero, showing better agreement after bias correction. While the mean bias is almost zero for Y polarization after bias correction, there is still a residual bias remaining of about 4 K at X polarization. This reflects the limitations of the CDF approach to account for all sources of monthly (climatological) biases in T$_B$, but it can also be influenced by bad data, especially data contaminated by RFI which were not tagged in the NRT product. There are still non-Gaussian tails present, which partly reflect the complexity of simulating L-band T$_B$ under a very heterogeneous land conditions with a radiative transfer model driven by a limited number of parameters and under very contrasting conditions.
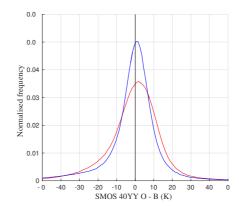

Figure 1: Normalized distribution of SMOS T$_B$ observations minus equivalent CMEM simulations before bias correction (red curve) and after bias correction (blue curve) for 40°X (left) and 40°Y (right).

2.3 The ECMWF surface and root-zone soil moisture analysis algorithm

The ECMWF soil moisture analysis system is composed of three main independent modules:

- The Hydrology-Tiled ECMWF Scheme for Surface Exchanges over Land (H-TESSEL),

- The Community Microwave Emission Model platform (CMEM) forward operator,

- The Simplified Extended Kalman Filter (SEKF) assimilation scheme,

The SEKF system combines screen level variables, ASCAT soil moisture retrievals and SMOS T_B observations with the HTESSEL-CMEM simulated top of the atmosphere T_B to adjust the soil moisture background values at analysis times. The three components are described in the following subsections.

2.3.1 H-TESSEL

H-TESSEL is the land surface scheme of the IFS used for operational weather prediction at ECMWF. H-TESSEL represents the time-space evolution of the most important hydrological and cold surface processes. It provides the background value of the land surface states for the atmospheric model integration. It also benefits from the global 4D-VAR data assimilation system used for the upper air analysis, as it provides high quality atmospheric conditions for land surface model integrations. H-TESSEL is a pointwise model that describes the soil water vertical diffusion using the Richards equation. On each grid point the vertical soil column is discretised into four layers (thicknesses of 7 cm, 21 cm, 72 cm and 1.89 m). The soil texture class used in H-TESSEL is extracted from the Food and Agriculture Organization (FAO)/ United Nations Educational, Scientific and Cultural Organization (UNESCO) Digital Soil Map of the World (DSMW) classification, which is available at a resolution of 5'x5' (about 10 km). The seven soil texture types used in H-TESSEL are coarse, medium, medium-fine, fine, very fine, organic and tropical organic. To interpolate to model target resolution, the dominant soil type is selected, with the advantage of preserving hydraulic properties when moving across various model resolutions. Each grid box in the model is divided into eight tiles (bare ground, low and high vegetation without snow, exposed snow, snow under high vegetation, interception reservoir, ocean/lakes, and sea ice). In each grid box two vegetation classes (high and low) are present. Twenty vegetation types, including deserts, ice caps, inland water and ocean, have been defined based on the US Geological Survey (USGS) classification of the Global Land Cover Characterization (GLCC, [Loveland et al., 2000]) data. Each vegetation type is characterized by a set of fixed parameters for the minimum canopy resistance, spatial coverage, and leaf area index, a sensitivity coefficient describing the dependence of the canopy resistance on water vapor deficit, and the root distribution over the soil layers. The fraction of a grid box covered by each of the tiles depends on the type and relative area of low and high vegetation, and the presence of snow and intercepted water.
An extensive description of the H-TESSEL land surface model is available in [Balsamo et al., 2009].

2.3.2 CMEM

CMEM is the ECMWF forward model operator for low-frequency passive microwave T_B in the range from 1 to 20 GHz ([Drusch et al., 2009a, de Rosnay et al., 2009]). It provides a model equivalent of the observed SMOS T_B at the top of the atmosphere, which is directly compared to the SMOS observed T_B at the time of the observation. CMEM input fields are provided by H-TESSEL integrations,

along with a monthly value of Leaf Area Index (LAI) per type of vegetation (based on a MODIS climatology, [Boussetta et al., 2013]) and other auxiliary land parameters as soil texture or water fraction. CMEM physics is based on the parameterisations used in the L-Band Microwave Emission of the Biosphere ([Wigneron et al., 2007]) and Land Surface Microwave Emission Model ([Drusch et al., 2001]). It is structured in four different modules for the soil, vegetation, snow and atmospheric contributions to the total microwave emission components. For each module, different parameterisations are available. The skill of CMEM to accurately represent the soil emission under different conditions is documented in the studies of [Drusch et al., 2009a], using L-band observations from the NASA Skylab mission in 1973-1974, [de Rosnay et al., 2009] using C-band observations provided by the AMSR on Earth Observing System (AMSR-E) on the NASA's AQUA satellite over the AMMA area in West Africa, and [Muñoz-Sabater et al., 2011] using in situ L-band observations of the SMOSREX (Soil Monitoring Of the Soil Reservoir Experiment) site in South-West France. In this study, the key parameterisations of [Wigneron et al., 2007] for the vegetation opacity contribution, in combination with the [Wang and Schmugge, 1980] dielectric model, the [Wigneron et al., 2001] for the soil roughness effect and the [Pellarin et al., 2003] parameterisation for the atmospheric contribution, were used. They were selected based on the minimum Root Mean Squared Difference (RMSD), minimum mean bias (MB) and best correlation (R) values of the simulated T$_B$ with the reprocessed SMOS dataset for the whole period 2010-2011 ([de Rosnay et al., 2018]). This combination of parameterisations is also used operationally at ECMWF since 19 November 2013 for monitoring purposes ([Muñoz-Sabater et al., 2014a]).

2.3.3   SEKF

The ECMWF soil moisture analysis uses the SEKF methodology. It is based on a point-wise EKF which combines a background state, screen level variables (2 m temperature and relative humidity) and satellite observations to obtain a soil moisture state of better quality than the pure model based estimation.

The soil moisture increment $\Delta \mathbf{x}(t_i)$ applied to the background vector $\mathbf{x}^b(t_i)$ at time t_i, grid point by grid point to obtain the analysis, is:

$$\Delta \mathbf{x}(t_i) = \mathbf{K}_i [\mathbf{y}^o(t_i) - H_i(\mathbf{x}^b)]$$

The superscripts b and o stand for background and observations, respectively, $\mathbf{x}$ is the model state vector, $\mathbf{y}$ the observation vector and H the non-linear observation operator relating observation and model equivalent. In this study, the model state vector has dimension $n = 3$, and it is composed of the soil moisture of the three top soil layers of H-TESSEL, whereas the observation vector is composed of 2 m temperature, 2 m relative humidity, ASCAT soil moisture retrievals and SMOS T$_B$ observations. The Kalman gain matrix $\mathbf{K}_i$ weighs the uncertainties assigned to the model background and the observations, and is computed at time t_i as:

$$\mathbf{K}_i = [\mathbf{B}^{-1} + \mathbf{H}_i^T \mathbf{R}^{-1} \mathbf{H}_i]^{-1} \mathbf{H}_i^T \mathbf{R}^{-1}$$

where $\mathbf{H}_i$ is the linearised version of the observation operator, $\mathbf{B}$ is the static error covariance matrix associated with the model state vector $\mathbf{x}^b$ and $\mathbf{R}$ is the observation error covariance matrix. In its operational version, the $\mathbf{R}$ matrix is static. However, since SMOS data were incorporated in the observation vector and, in this study, the uncertainty of each SMOS T$_B$ observation is proportional to its specific radiometric accuracy (see section 2.3.4), the $\mathbf{R}$ matrix becomes variable in space along the assimilation

window.

The Jacobian of the observation operator at time i, $\mathbf{H}_i$, provides information of the model 2 m temperature, 2 m relative humidity, ASCAT soil moisture retrievals and SMOS T_B sensitivity to small perturbations ($\delta \mathbf{x}_j$) of the top three j soil moisture layers. For the experiments described in this paper, $\mathbf{H}_i$ is:

$$\mathbf{H}_i = \frac{\delta \mathbf{y}_i}{\delta \mathbf{x}_j}$$

At ECMWF, $\mathbf{H}_i$ is numerically solved in finite differences, by forcing small $\delta \mathbf{x}$ perturbations of the background state vector, one for each element of the control state vector. This approach has the main advantage that tangent and linear models are not required, at the expense of a larger computational cost, but not prohibitive due to the low dimension (n=3) of the control vector. The optimal amplitude of the soil moisture perturbations for the linearisation of H, when only screen variables are assimilated, is documented in [Drusch et al., 2009b], whereas [Muñoz-Sabater, 2015] found similar values when SMOS T_B data were added to the control vector.

Finally, the nonlinear equations of the land surface scheme (described as the M operator) are used to make the new analyzed state vector $\mathbf{x}^a(t_i)$ evolve between time t_i and t_{i+1} according to:

$$\mathbf{x}^b(t_{i+1}) = M_{i \rightarrow i+1}[\mathbf{x}^a(t_i)]$$

2.3.4 SEKF setup and quality control

The success of the SEKF assimilation scheme depends on the accurate specification of $\mathbf{B}$, $\mathbf{R}$ and $\mathbf{H}$, as well as on different quality control checks to ensure that only good quality observations are used. Following [Muñoz-Sabater, 2015] the maximum perturbation of soil moisture permitted to linearize the Jacobian matrix of the observation operator was set to $0.01\,m^3 m^{-3}$. For this perturbation value, an absolute value of $250\,K/m^3 m^{-3}$ was found to be the maximum realistic sensitivity of model T_B to soil moisture variations. Negative values larger than $250\,K/m^3 m^{-3}$ were observed in the interface between snow and snow free areas and these observations are discarded. For the SMOS component of the Jacobian matrix, most grid points show negative values, reflecting the fact that, in general, an increased amount of water in the soil decreases the soil emissivity.

The observations are subjected to several quality checks; if the innovation (observations minus background) in observation space is larger than 20 K for T_B, then the observation is rejected. The same applies for 2 m temperature innovations larger than 5 K, 2 m relative humidity innovations larger than 20% and ASCAT soil moisture innovations larger than $0.1\,m^3 m^{-3}$. These values are currently used in operations and they are based on long-term statistics between modeled and observed values. Finally, soil moisture increments larger than $0.1\,m^3 m^{-3}$ are not applied to the background fields, as they are considered too large and not realistic.

Concerning the model and observation uncertainties, the covariance matrix of the observations $\mathbf{R}$ was assumed to be diagonal, with standard deviation of screen level parameters $\sigma_T = 1$ K and $\sigma_{RH} = 4\,\%$, whereas the ASCAT soil moisture retrieval error was set to $\sigma_{ASCAT} = 0.05\,m^3 m^{-3}$. These previous single values are probably not optimal for all the ranges of temperatures, humidities and soil moisture, however in this study they are used as in the operational ECMWF system. For SMOS observations a dynamical model error was set as $\sigma(T_B) = 6 + \alpha \cdot \text{rad\_acc}$, with rad_acc the pure radiometric accuracy of each individual pure polarised angular observation and α an inflation paramater. Based on long-term innovation statistics α was calibrated to be equal to 3. Thus the minimum error assigned to SMOS T_B observations

is around 10 K and acknowledges the fact that the radiometric accuracy, although an objective measure of the observation error, does not account for all sources of error, including the representativeness error and forward model uncertainties. Other studies used observation errors of the same magnitude ([de Lannoy and Reichle, 2016b, de Lannoy and Reichle, 2016a]). The assumption of a diagonal observation error covariance matrix also implies that there is no correlation between screen-variables, ASCAT retrievals and the different incidence angles of SMOS observations. However, there exists at least a certain level of horizontal error correlation among the different multiangular SMOS observations at each model grid point. As in this study the resolution of the analysis matches the resolution of the raw SMOS observations, we make the hypothesis that this assumption will not significantly impact the analysis. Investigating the effect of horizontal correlations between observation errors is necessary, but it is out of the scope of this paper.

A 3D-background error matrix (3D-**B**) based on [Muñoz-Sabater et al., 2018] was used to describe the uncertainty of the soil moisture background. The variance of each model soil moisture layer is assumed to be dependent on the water holding capacity (WHC), defined as the difference between soil moisture at field capacity (w_{fc}) and wilting point (w_{wp}). This means that the background error has an horizontal dependency as WHC depends on soil texture too. In H-TESSEL the WHC varies between $0.151 \, m^3 m^{-3}$ for loamy texture-type soils to $0.396 \, m^3 m^{-3}$ for organic soils. It is also assumed that errors in the top layer are more sensitive to precipitation and forcing errors. Thus, the background error is simply defined as being proportional to 10%, 5% and 5% of the WHC for the top, medium and deepest layer of the analysis, respectively. This is equivalent to assuming the model soil moisture errors vary between 1.1 mm for loamy soils to 2.8 mm for organic soils integrated over the top 7 cm of the top layer, or between 8.1 mm and 21.2 mm integrated over the top meter of soil. If the background error was maintained constant as in operations (1% volumetric error of the background value) this would be equivalent to considering the error varying from 0.11 mm to 0.31 mm for a medium type soil and for the top soil layer, or from 1.51 mm to 4.39 mm for the root-zone. This would mean a clearly more conservative approach, as the background error would be significantly reduced giving more weight to the model first guess.

Finally, the full observing system was used for the upper air analysis, as set in operations, aiming at providing the best possible quality of the atmospheric and related land surface conditions for the surface integrations.

2.4   Description of experiments

Six experiments of a duration of five months each, spanning from 1 May to 30 September 2012, and six more covering the same period but in 2013, were run. These years and this season was selected because SMOS T$_B$ reprocessed data were available at that time and because the Northern Hemisphere evapotranspiration rates are stronger during this period of the year, leading to stronger sensitivity to the assimilated data both in the soil and the atmosphere. The first experiment (**SLV**) assimilates 2 m temperature and 2 m relative humidity pseudo-observations from synoptic stations at synoptic times (00, 06, 12 and 18UTC), in assimilation windows of 12 h, which is similar to the assimilation window used in the ECMWF atmospheric 4D-VAR system. An open loop experiment (**OL**) was also used, i. e., an experiment where the soil moisture analysis step is skipped, and thus the soil moisture state is evolving in time with the atmospheric forcing providing the only constraint for the land-surface model. The other four experiments used a combination of screen level variables and remote sensing data, as follows:

- **SMOS**; Assimilates only SMOS T$_B$,

- **ASCAT**; Assimilates only ASCAT soil moisture index retrievals,

- **SMAS**; Assimilates SMOS T$_B$ and ASCAT soil moisture index retrievals,

- **SLVSMAS**; Assimilates all sources of data, i.e., 2 m temperature and 2 m relative humidity, SMOS T$_B$ and ASCAT soil moisture retrievals.

The first 15 days of the experiments were discarded from the evaluation as they were considered as a spin-up period to reach hydrological balance, as the introduction of a new type of observations may take time to adjust. The experiments were run at global scale and the model horizontal resolution was set to spectral truncation TL511, approximately 40 km.

The components of the **B** error matrix in the experiments above depend on the soil texture and the depth of the soil layer. This is different from the operational configuration, in which background variances are set to a fixed value of $\sigma^2(SM) = 0.01^2 \, m^3 m^{-3}$ for all dimensions. In order to study the sensitivity of the forecast skill to this new definition of the **B** error matrix, the **SLV** and **SMOS** experiments were repeated in 2013 but using the operational **B** fixed matrix. Results are presented in section 3.7. Table 1 summarizes all the experiments carried out in this study.

expt name	SLV	ASCAT	SMOS	2012	2013	B-fix	3D-**B**
OL				✓	✓		
SLV	✓			✓	✓		✓
ASCAT		✓		✓	✓		✓
SMOS			✓	✓	✓		✓
SMAS		✓	✓	✓	✓		✓
SLVSMAS	✓	✓	✓	✓	✓		✓
SLV(B$_{fix}$**)**	✓				✓	✓	
SMOS(B$_{fix}$**)**			✓		✓	✓	

*Table 1: Experiments carried out in this study; Left column is the name of the experiment and top row is the type of assimilated observation (screen level variables (SLV), ASCAT soil moisture retrievals and/or SMOS T$_B$), year of experiment (2012 and/or 2013) and the definition of the background **B** error matrix (static variances (**B**$_{fix}$) or depending on soil texture and depth (3D-**B**)).*

2.5 Evaluation strategy

The quality of the soil moisture analysis of each experiment was evaluated by comparing the analyses to independent in situ observations available through the International Soil Moisture Network (ISMN) database. Available observations from the following networks were used:

- 12 automated weather stations of the SMOSMANIA network in South-West of France ([Calvet et al., 2007]),

- 177 stations belonging to the NRCS-SCAN network in the US ([Schaefer et al., 2007]),

- 114 stations of the U.S. Climate Reference Network National from the Oceanic and Atmospheric Administration's National Climatic Data Center (USCRN NOAA's NCDC, ([Bell et al., 2013])),

- 19 stations from the REMEDHUS network, in the Duero Basin of Spain ([Martinez-Fernandez and Ceballos, 2003]),

The best spatial coverage is found in the US. In this evaluation exercise, in situ data are considered the ground "truth", despite that in situ observations are also affected by errors, depending on the method used to provide measurements and representativeness errors. We refer the reader to [Dorigo et al., 2011] for more information on each network. The metrics selected to evaluate the analyses are the correlation time series coefficient (R) and the unbiased Root Mean Square Difference (ubRMSD). The latter is obtained after removing the (static) long term mean bias between simulated soil moisture and ground station observations. These metrics were applied to both the surface soil moisture (top 7 cm of soil) and the root-zone (0-100 cm of soil), the latter being the variable of interest for most hydrological and climate applications, as it controls processes such as the evapotranspiration. In order to avoid stations with a large seasonal amplitude artificially increasing the correlation time series coefficient, the anomaly correlation (an_R) was also computed by removing the soil moisture climatology from simulations and observations. The difference from the mean was produced for a sliding window of five weeks (if there are at least five measurements in this period), and the difference scaled to the standard deviation.

For the root-zone, the averaged vertical value of in situ observations at 5, 10, 20, 30, 50 and 100 cm over the SCAN and USCRN networks in the US was compared to the averaged soil moisture analyses of the three first layers of the soil (0-100 cm), weighted by the layer thickness. For the SMOSMANIA network the procedure was similar, but observations are only available up to a depth of 30 cm, however they are representative of the root-zone ([Albergel et al., 2009]). The results are presented in the right panel of Table 2. Note that an_R was computed only for the top soil moisture layer, as it provides information on the short term variability, which is less pronounced in the root-zone. In addition, the skill of the land surface model to predict soil moisture up to 5 days with an initial state resulting from the soil moisture analysis step was also evaluated through comparison to observations of the USCRN network. The soil moisture validation database was harmonized using the p-value test (a measure of the correlation significance). Only cases where the p-value was below 0.05 (i.e., 95% of probability that the correlation coefficient is not a coincidence) for the analysis were retained. Stations with non significant R values were excluded from the computation of the network average metrics. Confidence intervals were provided using the Fisher Z transform as in [Draper et al., 2012] and [Albergel et al., 2013].

The sensitivity of temperature and humidity at screen level (cooling or warming) to the new analyses was also investigated and the forecast error of these variables evaluated by comparing to their own analysis. In addition, four of the lowest pressure atmospheric levels (700, 850, 925 and 1000 hPa) were selected to evaluate the influence on the skill of forecasted atmospheric variables, including air temperature, humidity, wind and geopotential. The metrics investigated were the forecast error and anomaly correlation, both normalized by the control experiment. As reference the best possible analysis available was used, which was the operational analysis. Statistical significance, where given, is based on [Geer, 2016]. Error bars come from a Student's T-test on the paired differences with two additional corrections: autocorrelation correction based on autocorrelation tables derived from [Geer, 2016] and the autogressesion AR(2) model and multiplicity correction of [Geer, 2016], which is a Sidak correction assuming 4 independent tests per experiment.

3   Results

3.1   Observations used in the analysis

Fig. 2a shows the number of SMOS T$_B$ observations at 30°, 40° and 50° respectively, in X polarization, available for assimilation in the ECMWF SEKF, for a period of 30 days in July-August 2013, after applying the quality control and thinning steps explained in section 2.1.3. As expected, due to the polar orbit of the SMOS satellite with shorter revisit time at higher latitudes, the number of observations increases with the latitude in the boreal summer months, with few areas covered by snow and ice. This figure also shows stripes that are due to some areas missing part of a cycle as a consequence of using only the alias-free zone, but it also reflects the winter conditions of the Southern Hemisphere, rejecting observations in New Zealand, South-East Australia, South Africa and Patagonia. The very low number of observations available in the Andes, the Alps, the Himalayas and some areas of the Rockies are due to filtering steps based on snow, frozen soils and high orography. Fig. 2b shows the standard deviation of the background departures using these observations. The largest variability is found either in areas very sensitive to soil moisture variations, with large annual amplitude of T$_B$, such as the Great Plains of North-America, or in parts of the Middle-East and Asia, the latter two areas are often strongly impacted by RFI. These observations are in addition subjected to various SEKF quality checks. Fig. 2c shows the percentage of SMOS observations that were assimilated after the SEKF quality checks. It is observed that the SEKF filters remove up to 90% of observations in the Middle-East or some zones of China, due to large disagreements with the simulated T$_B$ by CMEM. This reflects the limitations of the RFI flagging used to detect contaminated measurements. The SEKF quality control acts as an additional filter preventing poor observations from influencing the analysis. Fig. 2c also shows that a lot of observations were removed in very high latitudes, especially in Canada, where the CMEM model T$_B$ is not accurate in a mixed soil layer of liquid water and snow. The map of the standard deviation of the background departures after the SEKF filters were applied (Fig. 2d) shows significantly more realistic values compared to Fig. 2b. They can be as large as 10 K, showing areas that potentially contain rich information on soil moisture variations. The number of SLV observations available for the soil moisture analysis, after the SEKF quality control, is shown in Fig. 3a. As explained in section 2.1.1, previous to use in the SEKF, a 2D-OI scheme is applied to 2 m temperature and 2 m relative humidity observations, making SLV pseudo-observations available at each land grid point and each day at 00, 06, 12 and 18UTC. This means approximately 240 pseudo-observations available for 30 days at each model grid point (Fig. 3a). The SEKF rejects some of these pseudo-observations in areas with high information content of soil moisture, such as the Sahel transition zone, where indeed the SMOS observations show very good sensitivity. In Fig. 3b, much less ASCAT soil moisture retrievals are available for assimilation, a maximum of 2 observations per assimilation window. Tropical forests and high-density vegetation mask C-band observations, and this is reflected in Fig. 3b, with no retrievals available in these areas.

In summary, the adjustment of the background soil moisture value over the whole assimilation period will be influenced by a larger number of observations (and pseudo-observations) of air temperature and air humidity at screen level. However when a grid point is located in the satellite swath of SMOS, the number of SMOS T$_B$ observations will dominate over screen observations and ASCAT retrievals (six observations [three angles and two polarisations] vs. four screen level observations or two ASCAT retrievals) for the analysis of soil moisture.
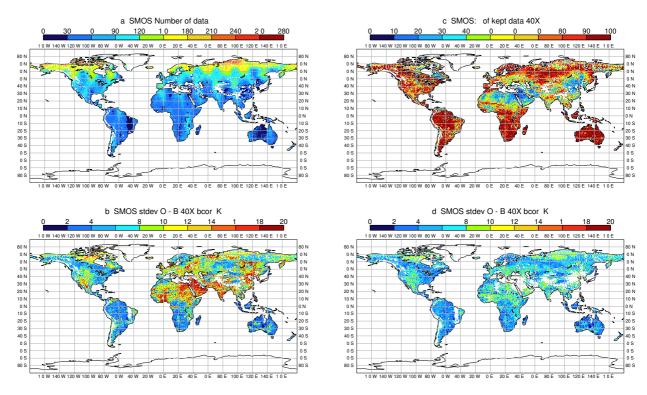
Figure 2: a) Number of SMOS T$_B$ observations in X polarization available for assimilation after quality control and the filters applied in section 2.1.3, b) Standard deviation of the background departures with observations used in a), c) Percentage of remaining assimilated SMOS T$_B$ observations after the SEKF quality control steps, d) Standard deviation of the background departures with observations used in c). Values are calculated for a 30-day period in July-August 2013.
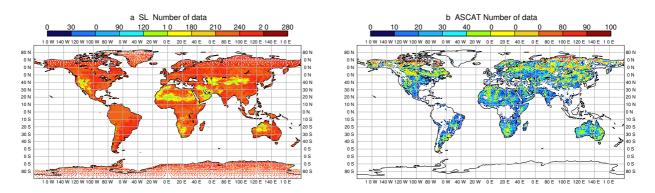

Figure 3: Number of a) screen level observations (2 m temperature and 2 m relative humidity) and b) ASCAT soil moisture retrievals available for analysis after the SEKF quality control. Values are for the same 30-day period as in Fig. 2.
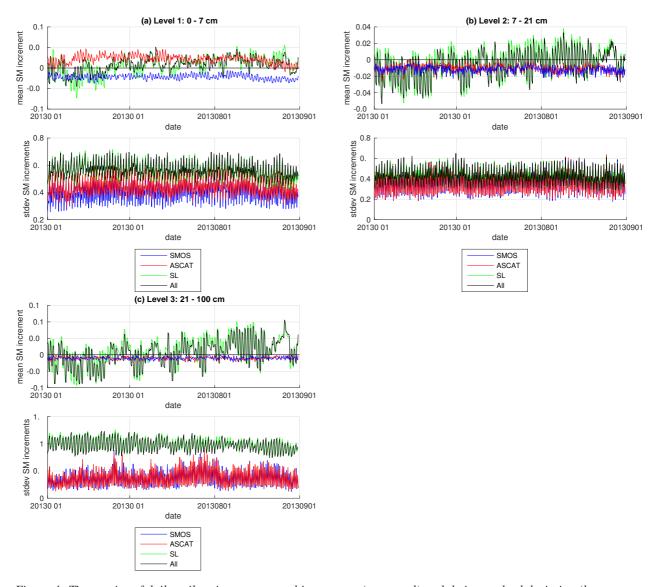
Figure 4: Time series of daily soil moisture averaged increments (top panel) and their standard deviation (bottom panel) for the a) 0-7 cm, b) 7-28 cm and c) 28-100 cm, soil layers. Units are mm/day.

3.2   Soil moisture increments

Fig. 4 shows the time series of the daily averaged soil moisture increments over land, and their daily averaged standard deviation, for the **SLV**, **ASCAT**, **SMOS** and **SLVSMAS** experiments. Values are shown separately for the top three layers of the H-TESSEL model.

This figure shows that the mean increments of the SMOS and ASCAT configurations, for the top layer, are numerically comparable to those of the **SLV** experiment. However, one should bear in mind that contrary to the screen level variables, the assimilated SMOS T_B and ASCAT L2 retrievals are assimilated only over the satellite track on 12 h windows. Hence, the daily averaged increments of **ASCAT**, **SMOS** and **SMAS** over all land grid points is reduced by those land grid points without any satellite observation, where increments will be zero. Therefore, in relative terms, the top soil layer increments of the **SMOS** and **ASCAT** experiments are larger than those of **SLV**. This is what makes remote sensing data very interesting to adjust model soil moisture at global scale, as they show strong sensitivity to soil moisture
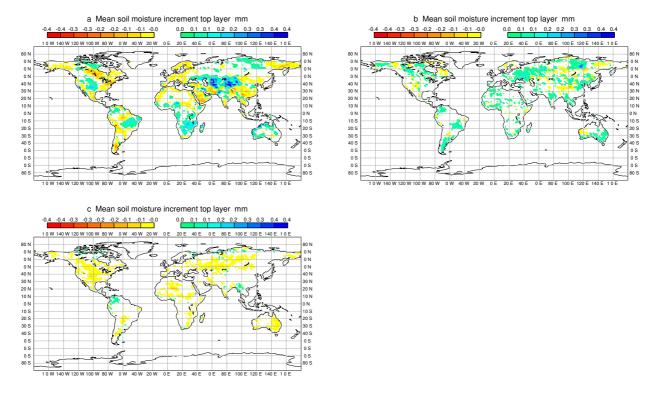
*Figure 5: Time-averaged soil moisture increments (in mm) from May-Sept 2013 for the a) **SLV**, b) **ASCAT** and c) **SMOS** experiments and for the top 7cm of the soil.*

variations in the top first cm of the soil layer. For the top layer **SMOS** has a clear trend to, on average, dry the soil of a wet biased model (see for ex. soil moisture evaluation of [Albergel et al., 2012]). The drying is moderate and it occurs in areas mainly identified as 'hot spots', as the Great Plains of US, Sahel, areas of Eurasia and East of Australia (see the time-averaged top soil moisture increments in Fig. 5c). As it will be presented in section 5, this soil drying is in good agreement with in situ soil moisture observations in the US. On the other hand, the assimilation of ASCAT soil moisture retrievals tends to add water to the soil over larger areas (Fig. 5b). The time series standard deviation of the **SLV** mean increments is near 50% larger than that of the **SMOS** and **ASCAT**, which is due to larger absolute increments, as shown in Fig. 6. Their temporal and spatial distribution is also more variable in the **SLV** experiment, because it tries to keep screen level errors at a minimum. In the second and third land model layers, **SMOS** also tends to dry the reservoir, and it is consistent and of similar magnitude than the **ASCAT** increments (see Fig. 4b and c). For both **SMOS** and **ASCAT** experiments, increments for the third layer integrated over its thickness (72 cm) are relatively very small compared to those of **SLV**, reflecting the small penetration depth of low frequency microwaves. Although screen temperature and humidity observations also reduce sensitivity with depth, they still show larger sensitivity than satellite data through perturbed forecasts of soil moisture.

3.3 Soil Moisture evaluation

Table 2 presents the ubRMSD, R and an_R of the experiments analyses compared to ground observations for several networks with available data, both for the surface layer (top 7 cm of the soil) and the root-zone (top first meter of soil for US networks or top 30 cm for the SMOSMANIA network). In order
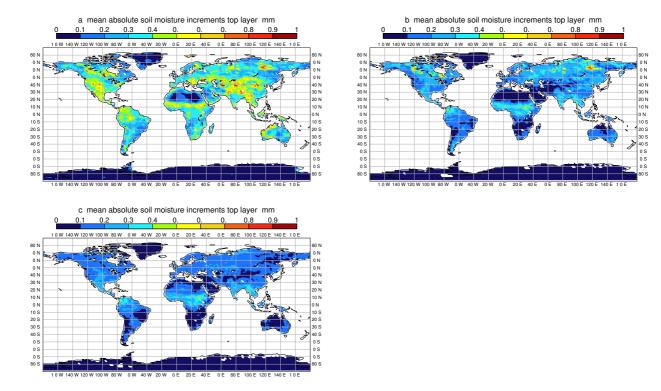
*Figure 6: Time-Averaged absolute soil moisture increments (in mm) from May-Sept 2013 for the a) **SLV**, b) **ASCAT** and c) **SMOS** experiments and for the top 7cm of the soil.*

to check for consistency, averaged values are shown separately for the period May-September 2012 and 2013. The validation was carried out on a daily basis and only at the analysis time, i.e, each day the mean in situ soil moisture value per each station at 00, 06, 12 and 18UTC was computed and compared to the corresponding daily mean analyses at the same four synoptic times. The number of stations with statistically significant values for all the period of study (according to the p-value test) is also included in Table 2.

		surface				root-zone		
		ubRMSD	R	an_R	N	ubRMSD	R	N
REMEDHUS	OL	0.053	0.72 (0.12)	0.42 (0.16)	17			
		0.049	0.72 (0.12)	0.50 (0.12)	15			
	SLV	0.052	0.74 (0.08)	**0.56 (0.16)**	17			
		0.049	0.68 (0.07)	**0.55 (0.12)**	15			
	ASCAT	**0.045**	0.69 (0.12)	0.45 (0.13)	17			
		0.047	0.68 (0.10)	0.42 (0.09)	15			
	SMOS	0.049	**0.77 (0.12)**	0.54 (0.13)	17			
		0.050	**0.73 (0.14)**	0.46 (0.09)	15			
	SMAS	0.048	0.72 (0.09)	0.49 (0.13)	17			
		0.046	0.71 (0.05)	0.42 (0.10)	15			
	SLVSMAS	0.055	0.74 (0.08)	0.48 (0.11)	17			
		0.048	0.66 (0.07)	0.45 (0.11)	15			
SMOSMANIA	OL	0.049	0.78 (0.08)	0.62 (0.11)	11	0.030	0.85 (0.09)	11
		0.049	0.84 (0.08)	0.62 (0.14)	10	0.032	0.89 (0.06)	10
	SLV	0.048	0.75 (0.12)	0.61 (0.10)	11	**0.029**	0.82 (0.08)	11
		0.049	0.83 (0.11)	0.55 (0.14)	10	**0.031**	0.89 (0.06)	10
	ASCAT	0.047	**0.80 (0.06)**	0.64 (0.15)	11	0.035	0.84 (0.06)	11
		0.052	0.85 (0.08)	0.59 (0.12)	10	0.034	**0.90 (0.06)**	10
	SMOS	**0.044**	**0.80 (0.09)**	**0.65 (0.12)**	11	0.031	0.86 (0.12)	11
		0.049	**0.86 (0.09)**	**0.62 (0.10)**	10	0.032	**0.90 (0.07)**	10
	SMAS	0.046	**0.80 (0.07)**	**0.65 (0.12)**	11	0.031	0.86 (0.08)	11
		0.050	0.84 (0.10)	**0.62 (0.12)**	10	0.032	**0.90 (0.06)**	10
	SLVSMAS	0.047	0.74 (0.09)	0.64 (0.14)	11	0.031	**0.89 (0.09)**	11
		0.047	0.80 (0.09)	0.59 (0.11)	10	**0.031**	0.88 (0.10)	10
USCRN	OL	0.049	0.68 (0.04)	0.62 (0.04)	63	0.030	0.80 (0.06)	63
		0.052	0.70 (0.06)	0.63 (0.03)	61	0.027	0.78 (0.05)	61
	SLV	0.054	0.64 (0.08)	0.56 (0.04)	63	0.031	0.73 (0.06)	63
		0.055	0.66 (0.03)	0.59 (0.05)	61	0.029	0.68 (0.08)	61
	ASCAT	**0.047**	0.68 (0.05)	0.62 (0.06)	63	0.030	0.77 (0.05)	63
		0.050	0.72 (0.04)	0.61 (0.04)	61	0.029	0.77 (0.06)	61
	SMOS	0.048	**0.72 (0.04)**	**0.63 (0.04)**	63	0.030	**0.81 (0.07)**	63
		0.049	**0.73 (0.04)**	**0.65 (0.03)**	61	**0.026**	**0.80 (0.06)**	61
	SMAS	0.050	0.69 (0.04)	**0.63 (0.04)**	63	0.031	0.79 (0.05)	63
		0.049	0.72 (0.04)	0.64 (0.06)	61	0.027	0.79 (0.06)	61
	SLVSMAS	0.054	0.65 (0.06)	0.57 (0.06)	63	**0.029**	0.74 (0.07)	63
		0.056	0.66 (0.04)	0.61 (0.05)	61	0.031	0.73 (0.04)	61
SCAN	OL	0.054	0.61 (0.05)	0.59 (0.04)	80	0.033	**0.63 (0.14)**	80
		0.053	0.68 (0.03)	0.60 (0.04)	107	0.029	0.71 (0.06)	107
	SLV	0.056	0.59 (0.05)	0.51 (0.06)	80	0.032	0.54 (0.09)	80
		0.059	0.64 (0.04)	0.60 (0.04)	107	0.031	0.66 (0.06)	107
	ASCAT	0.054	0.62 (0.05)	0.59 (0.04)	80	0.032	0.60 (0.11)	80
		0.052	**0.70 (0.03)**	0.60 (0.06)	107	0.029	0.70 (0.04)	107
	SMOS	0.054	0.62 (0.05)	0.58 (0.03)	80	0.031	0.62 (0.05)	80
		0.053	**0.70 (0.03)**	**0.62 (0.04)**	107	0.028	**0.73 (0.04)**	107
	SMAS	**0.053**	**0.64 (0.05)**	**0.61 (0.06)**	80	0.032	0.62 (0.11)	80
		0.052	0.67 (0.04)	**0.62 (0.03)**	107	**0.026**	0.71 (0.04)	107
	SLVSMAS	0.058	0.59 (0.05)	0.54 (0.06)	80	**0.030**	0.58 (0.07)	80
		0.055	0.66 (0.04)	0.60 (0.04)	107	0.030	0.68 (0.04)	107

Table 2: *Network averaged unbiased Root Mean Square Error Difference (ubRMSD) ($m^3 m^{-3}$), time series correlation (R) and anomaly correlation (an_R) between soil moisture analyses and ground observations. For each experiment, the top line is the average over the period May-Sept. 2012, and second line for the equivalent period in 2013. Values in parenthesis for R and an_R represent the estimated uncertainty. Bold-face values are the numerically best scores for each year and metric. N represent the number of stations with statistically significant values for all the period under study.*

For surface soil moisture and for all the evaluation networks and both years under study, the analysis of the experiments assimilating only satellite data (**SMOS**, **ASCAT** and **SMAS**) obtained the best correlation with in situ averaged values. In particular, **SMOS** analyses were consistently the best over the REMEDHUS, SMOSMANIA and USCRN networks for both 2012 and 2013. Only the combination of SMOS and ASCAT data (**SMAS** experiment) obtained the best correlation in 2012 over the SCAN network. This result highlights the added value of remotely sensed data to obtain information of the relative temporal variability of the shallow soil moisture time series, and in particular of passive L-band microwaves given their larger sampling depth and lower sensitivity to vegetation. The analyses of the **SLV** experiment had the poorest correlation with in situ data. The fact that correlation values for **SLV** are worse than those of the **OL** evidences the problems of screen observations in realistically adjusting soil moisture over a long period in a system originally designed to make the soil state respond to errors of temperature and humidity at screen level. The uncertainty estimation calculated through the Fisher Z transform is larger for the SMOSMANIA and REMEDHUS stations, as the number of stations with significant correlation values is much reduced compared to the Northern American networks. The results for the anomaly correlation show lower skill of the analyses to catch the short term variability, as the seasonal cycle is not influencing this metric, but they also show quite similar results as for the correlation coefficient, i.e., the ability of satellite data to provide dynamic information of soil moisture more accurately than screen level observations. The exception is the REMEDHUS network. It should be noted that for soil moisture validation the period under study is relatively short, and therefore the confidence intervals of the correlation metrics calculated through the Fisher Z transform are relatively large, making the results mostly statistically non significant. The ubRMSD results show relative small differences among the experiments, mostly below $0.01\,m^3m^{-3}$. The assimilation of SMOS and/or ASCAT data reduces the ubRMSD up to $0.044\,m^3m^{-3}$, consistently showing the lowest values for the **SMOS**, **ASCAT** and **SMAS** analyses, although they alternate depending on the network and the year. In general, the **SLV** experiment obtained the largest values of ubRMSD, up to $0.059\,m^3m^{-3}$, showing again the difficulties of the system to keep realistic values of soil moisture when it relies only on screen temperature and humidity.

For the root-zone, only observations in USCRN, SCAN and SMOSMANIA networks were available. However, one should bear in mind that this validation exercise is not trivial, as in situ observations at only 5 different depths are considered to sample the first meter of soil. In general the correlation values are better than for the top layer because variability is lower at deeper depths, and these values are as high as 0.9. While in general the root-zone evaluation still provides the best correlations for the experiments assimilating satellite data, the difference with the **OL** are reduced. This is because the soil moisture information contained in SMOS and ASCAT data is mainly sensitive to the top few cms of the soil, and the influence (and increments) in deeper layers is reduced through perturbed forecasts. The **SLV** analyses also obtain the worst correlation values, suggesting a degradation of soil moisture when only screen information is assimilated. The ubRMSD is quite similar for all experiments, in all cases below $0.04\,m^3m^{-3}$ as a result of the lower variability of the water content in the root-zone reservoir.

3.4   Soil moisture forecasts

The evaluation of the soil moisture forecasts of **OL**, **SLV**, **SMOS** and **ASCAT** experiments against in situ stations from the USCRN network is shown in Fig. 7. Each 5-day forecast was started at 00UTC and initialized from the same day 00UTC surface analysis, and the forecast was compared with the observation at the forecast time. The period of forecasts spans from 15 May to 30 Sept. 2012 and 2013 combined. Fig. 7 shows the correlation coefficient and the ubRMSD of the forecasts compared to in situ data at five leading times, 24h, 48h, 72h, 96h and 120h. As expected, the quality of the forecast decreases with the lead time (lower correlation coefficient and greater ubRMSD) and the correlation and

biases tend to converge for longer lead times. The latter also shows that the memory of the better skill shown by the **SMOS** soil moisture forecasts, in terms of correlation with in situ stations, is maintained at least up to day 5, just ahead of **OL** and **ASCAT**. The comparison also shows **SLV** to obtain the weakest skill for all lead times and both metrics, which is consistent with the results analysis of the previous section. For the first 48 h, none of the experiments assimilating remote sensing data overperform the **OL** in terms of lowest ubRMSD.

Figure 7: Averaged correlation time series coefficient (left y-axis, black symbols) and ubRMSD (right y-axis, red symbols) between the soil moisture forecasts of OL, SLV, ASCAT and SMOS and in situ observations of the USCRN network. Values are an average over the periods 15 May to 30 Sept 2012 and 2013, combined.

3.5 Screen level variables and forecast error sensitivity to analyses

Figs. 8a and **b** show the sensitivity of 24h 2 m temperature forecasts to the soil moisture analyses of **SLV** and **ASCAT**. The reference experiment is the **OL**. The plots show averaged values over the period May-September 2012 and 2013 combined. Figs. 8c and **d** show similar plots for SMOS T_B assimilation at 12 h and 24 h forecast. As expected from section 3.2, the larger absolute increments of soil moisture in **SLV** have a largest influence on the forecast of 2 m temperature, cooling the atmosphere in large parts of Africa and Australia, Central Asia, Central North-America and Brazil, most of them at night-time, which is in good agreement with the top layer soil moisture increments of Fig. 5a. This cooling can be even larger than 2 K in some areas due to a warm summer model bias. On the contrary, warming patterns are observed in several parts of America, Europe and China. These complex large scale patterns of near surface air temperature biases vary depending on the season and the lead forecast time. Their origin is multiple and range from so diverse factors as an overestimation of turbulent mixing in a cloudy boundary layer to an overestimation of the thermal coupling between the surface and the uppermost surface layer. They are currently under investigation at ECMWF [Haiden et al., 2018]. In comparison to SLV assimilation, the small adjustment of the soil state produced in the **ASCAT** and **SMOS** experiments has a weaker effect on 2 m temperature forecasts at 24 h. ASCAT has a weak cooling effect in most areas,

(a) SLV-OL 24h fc.

(c) SMOS-OL 12h fc.

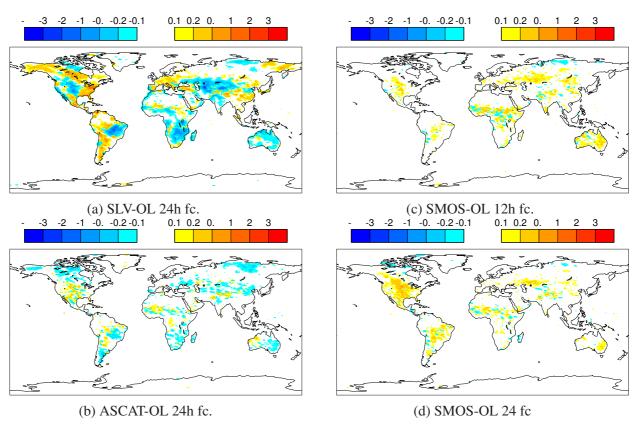(b) ASCAT-OL 24h fc.

(d) SMOS-OL 24 fc

*Figure 8: Sensitivity of 24 h screen level temperature forecast to the soil moisture analyses of a) **SLV**, b) **ASCAT**, and to **SMOS** soil moisture analyses at c) 12 h and d) 24 h forecast. The blue colour bar indicates cooling of 2 m temperature, and red colour bar warming of 2 m temperature. The reference experiment is the **OL**. Units are K.*

which is consistent with the slight positive soil moisture increments of the top layer. In contrast, the soil drying in SMOS has a clear warming effect on air temperature that is more marked during daytime. An interesting area is the Great Plains of Northern America, where an opposite signal is found between **SLV** and remote sensing data assimilation (warming the near-surface temperature). In this area the analyses of **ASCAT** and **SMOS** showed better agreement with in situ data. Fig. 9 shows the equivalent figures for the mean absolute forecast error differences. Negative values means that the absolute difference between the forecast and the own experiment analysis is reduced compared to the **OL** averaged over the period of study. The latter is a sign of smaller corrections of the background and better forecasts. As observed in Fig. 9a, **SLV** produces on average the largest reduction in 2 m temperature forecast errors. Despite a better match of soil moisture analyses with ground station data, the assimilation of remote sensing data has a very weak effect on screen level temperature. The same results are obtained for 2 m relative humidity forecasts (not shown).

(a) SLV-OL 24h fc.

(c) SMOS-OL 12h fc.

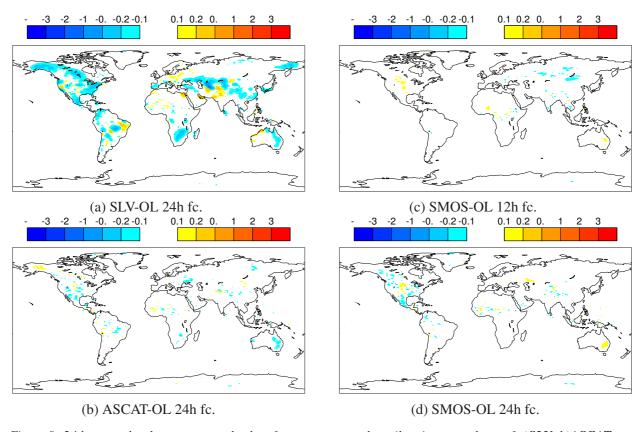(b) ASCAT-OL 24h fc.

(d) SMOS-OL 24h fc.

*Figure 9: 24 h screen level temperature absolute forecast error to the soil moisture analyses of a)**SLV**, b)**ASCAT**, and to **SMOS** soil moisture analyses at c) 12 h and d) 24 h forecast. The blue colour bar indicates reduction of forecast error (enhancement) and red colour bar increase of forecast error (degradation). The reference experiment is the **OL**. Units are K.*

3.6 Atmospheric forecast scores

Fig. 10 shows the root mean square (RMS) forecast error of air humidity normalized by the open loop reference RMS error. Scores are shown for the Southern Hemisphere extra-tropics (left column) and Northern Hemisphere (right) extra-tropics regions, and Tropics (20°S-20N) (middle), at four pressure levels in the boundary layer, from 1000 hPa pressure level (bottom row) to 750 hPa (top row), and up to 10 days forecast lead time. The skill is shown for the period 15 May to 30 Sept 2012 and 2013 combined, in total 276 samples were averaged using both 00UTC and 12UTC forecasts. Negative values indicate increase of skill in the prediction of a variable with respect to the **OL** prediction, whereas positive values indicate reduction of forecast skill. Error bars, based on [Geer, 2016], are overlapped to the averages and those crossing the zero line indicate non-significance from the statistical point of view. The main impact of the assimilation is found very close to the surface whereas the impact is reduced higher in the troposphere and progressively losing statistical significance. Indeed no impact at all is observed for pressure levels lower than 700 hPa (not shown). This result was expected as the primary effect of assimilating the data of these experiments is the change of the soil moisture state. In turn, the influence in the troposphere is complex and is not only driven by soil moisture changes, but by many other factors such as the meteorological conditions or the parametrized coupling strength between continental masses and the lower troposphere, making the assimiliation of SMOS T_B difficult to evaluate. The Northern Hemisphere extra-tropics, with the largest continental masses, is the zone where the assimilation of observations sensitive to soil moisture has the largest impact. In this region, adding screen level data to the control vector has a significant increase of the air humidity prediction skill, up to 3% in the first 48h, whereas this value can be up to 1.5% in the Southern Hemisphere. Assimilating only SMOS data has a small significant degradation in the Northern Hemisphere air humidity up to 0.3% for the first 3 forecast days, whereas it has a positive significant improvement up to 0.7% in the Southern Hemisphere. The main degradation signal comes from the Great Plains (not shown), which indeed is a region where the SMOS data assimilation has shown to be very positive for the initialization of the soil state when evaluated against independent in situ soil moisture data. This is also the region showing discrepancy between soil moisture increments (Fig 4a) and screen level temperature errors (Fig. 8a) for the **SLV** experiment. This points to an IFS model deficiency in respect to how surface fluxes respond to the soil moisture content. In this region an improvement of soil moisture by SMOS data assimilation is achieved at the expense of degrading atmospheric forecasts. Increasing realism of one surface process can leave the model exposed to errors in other associated processes. Research at ECMWF is ongoing to improve the realism of the IFS model surface layer and surface fluxes. For the **ASCAT** experiment the situation is just opposite than for **SMOS** but with even lower impact, whereas the compensating effect of combining ASCAT and SMOS data is reflected in more neutral scores in the **SMAS** experiment. Adding all observations to the control vector (**SLVSMAS**) has a very slight, but not statistically significant, positive effect on the first 48 h compared to the **SLV** scores. The situation in the Tropics is more neutral. Similar plots for air temperature can be found in the appendix (Fig. 15), with the main difference that scores are very neutral for the Southern Hemisphere extra-tropics. For **SLV** significant positive impact was also found in the Tropics and Northern Hemisphere extra-tropics in the low-level cloud cover, mean sea level pressure and geopotential height (see Figures 16, 17 and 18 in the Appendix).

3.7 Operational vs. 3D-B background error matrix

The results presented above are based on experiments where a 3D-**B** matrix was specified for the model background error (as described in section 2.3.4). This makes a difference with regards to the operational
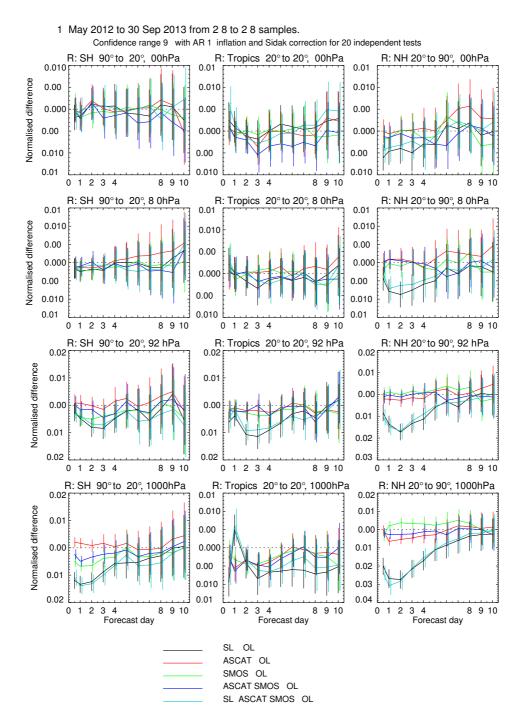
Figure 10: Normalized RMS forecast error of the lower troposphere air humidity for the Southern Hemisphere extra tropics region (left column), Tropics (middle column) and Northern Hemisphere extra-tropics (right column), and for the 700 hPa (top row), 850 hPa (second row), 925 hPa (third row) and 1000 hPa (bottom row) pressure levels. The black curve is for the SLV experiment, red curve for ASCAT, green curve for SMOS, dard blue for SMAS and light blue for SLVSMAS. All of them are compared (and normalized) to the OL experiment. The forecast period is May-Sept 2012 and 2013, combined.

set up where the **B** matrix is constant. It is important to test the implications of this change with respect to the operational configuration. Fig. 11 compares the scores of air temperature forecasts of the **SMOS** and

SLV assimilation experiments with the equivalent experiments but using the static **B** matrix as used in operations (**SLV**(**B**$_{fix}$) and **SMOS**(**B**$_{fix}$)). The reference here is the **SLV** 3D-**B** experiment, as described in section 2.4.
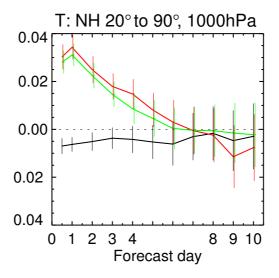

*Figure 11: Northern Hemisphere normalized RMS forecast error of air temperature at 1000 hPa level for the period May-Sept 2013. The reference experiment is **SLV** with 3D-**B** background error. Black curve is equivalent to **SLV** but with operational constant **B** matrix, red curve is **SMOS** experiment with 3D-**B** specification, and green curve corresponds to the **SMOS** experiment with constant **B** matrix.*

The significant negative values obtained by the black curve indicate that, by using a static **B** matrix, a small but significant increase in the skill of air temperature forecast of approximately 0.5% is obtained up to day 3. The positive values of the red and green lines indicate that compared to **SLV** assimilating SMOS T$_B$ only, degrades the skill of air temperature forecasts. Although non statistically significant, slightly better results are obtained by the **SMOS**(**B**$_{fix}$) experiment. This increase in skill is only observed in the Northern Hemisphere. Air humidity follows similar patterns (not shown). Fig. 12 shows the 2 m temperature component of the Gain matrix time series in both configurations. The net effect of specifying a 3D-**B** matrix is a decrease of the weight given to the background error (see discussion in section 2.3.4), and hence an increase of the gain component of 2 m temperature. Even if in absolute terms the gain values are small, they are significantly larger in the 3D-**B** configuration and consequently producing much larger increments as shown in Fig. 13. This result suggests that despite adding realism to the soil moisture background error, if in the ECMWF soil moisture analysis the weight assigned to the model background is reduced, then no extra benefits in predictive skill is obtained at longer periods. And this is true for the assimilation of only SMOS data or only screen level variables.
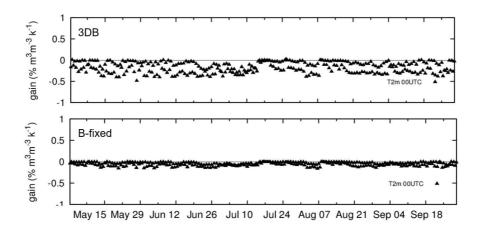
*Figure 12: 00UTC 2 m temperature component of the Gain matrix of the **SLV** experiments. Top) using a 3D-**B** description of the background error, bottom) using a **B** constant matrix as in the operational ECMWF system.*

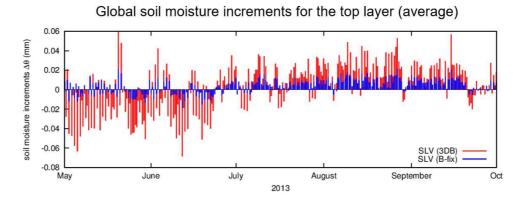Global soil moisture increments for the top layer (average)

*Figure 13: Daily averaged soil moisture increments assimilating screen level variables, using a 3D-**B** matrix of the background error (red bars) and the operational static **B** matrix (blue bars).*

4 Discussion

This is the first time that L-band T$_B$ data from a remote sensing platform has been implemented and used in the ECMWF land data assimilation scheme to constrain the temporal and spatial evolution of a very heterogeneous variable as soil moisture. The challenges in the implementation have been multiple, including the data management ([Muñoz-Sabater et al., 2012]), the varying uncertainty of the observations ([Muñoz-Sabater et al., 2014b]) and the optimal use of this information in the data assimilation system ([Muñoz-Sabater et al., 2018]). There are also other challenges associated with the modeling part, including the calibration of the radiative transfer model to accurately simulate T$_B$ under such diverse land conditions and limited soil information, as well as the consistency with boundary layer parameterization and coupling land-atmosphere aspects. This paper has shown the feasibility of implementing and assimilating SMOS data in the IFS, but it also exposed the many other challenges associated. In particular we acknowledge the complexity of making efficient use of these observations in a land surface model coupled with an atmospheric model, where the focus during the last decades has been on atmospheric forecast skill. Soil moisture has been used as a sink variable to absorbe errors in the model surface layer formulation.

The challenges involved also stand out when comparing the use of SMOS T$_B$ with the use of indirect screen level variables in the soil moisture analysis; Left panel of Fig. 14 shows the ratio of variances between SMOS T$_B$ observations and soil moisture background error values projected into observation space through the observation operator ($\mathbf{HBH}^T$), as a function of the linearized observation operator. Right panel is the equivalent for 2 m temperature. The red curve corresponds to a soil moisture background error of $\sigma(SM) = 0.01 \, m^3 m^{-3}$ (as currently set up in operations), whereas in the blue and green lines the error has been doubled and tripled, respectively. The observation error for SMOS T$_B$ has been fixed to a typical value of 15 K in our distribution, and 1 K for 2 m temperature. A grid point showing good sensitivity of T$_B$ to soil moisture variations has typical values of $\mathbf{H}$=150 $K/m^3 m^{-3}$. For the latter and $\sigma(SM) = 0.01 \, m^3 m^{-3}$, the ratio of variances is approximately 100, whereas it is approximately 4000 for 2 m temperature with a typical $\mathbf{H}$=1.5 $K/m^3 m^{-3}$. This is equivalent to assuming that, under these conditions, the observation error of 2 m temperature observations is approximately 65 times larger than the background error, whereas it is just 10 times for SMOS T$_B$. If the background error is doubled (tripled), then the ratio is 33 (22) for 2 m temperature and 5 (3.3) for SMOS T$_B$. This simple exercise shows that the relative weight assigned to SMOS T$_B$ observations in the analysis is larger than the relative weight given to screen level observations. To have both weights in the analysis equivalent (under the previous

conditions), the SMOS T$_B$ error should be almost 100 K, or decrease the error of 2 m temperature to 0.15 K. These values show that, the fact that SMOS observations are very sensitive to soil moisture variations (with large Jacobians components compared to 2 m temperature) also make them contribute with larger relative weight to the analysis. Therefore, despite the rich information content of soil moisture embedded in T$_B$, one has to be very careful when assimilating this type of data in an atmospheric model.
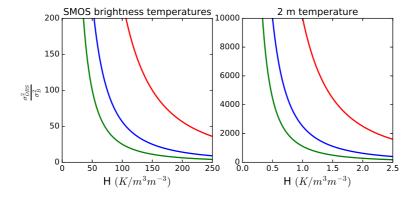

Figure 14: Ratio of variances between a) SMOS brightness temperatures observations and soil moisture background and b) 2 m temperature observations and soil moisture background values. The red curve corresponds to a soil moisture background error of $\sigma(SM) = 0.01\, m^3 m^{-3}$ (as currently set up in operations), whereas in the blue and green lines the error has been doubled and tripled, respectively.

There is no technical limitation preventing the assimilation of more incidence angles, however in our study the CDF monthly linear coefficients were optimized only for 30°, 40° and 50°, and X and Y polarizations. These angles are also less affected by angular noise and therefore of better quality ([Muñoz-Sabater et al., 2014b]). Besides, at intermediate incidence angles more data is available than at lower or larger angles, and they are separated at equal intervals of 10°. Yet, the combined use of these three angles also helps the radiative transfer model to account and discrimate the vegetation effect in the microwave signal. In our assimilation experiments, another consequence of such system is that the number of SMOS observations is so large that for a given grid point they can easily outnumber other conventional sources used for soil moisture analysis. Thus, again one has to be very careful when using these data in the assimilation system.

A final and non negligible challenge is the RFI contamination by sources emitting in the protected L-band frequency (1400-1427 MHz), which can substantially corrupt the measurement and render it unusable in some parts of the world. Although the SMOS T$_B$ used in this study for assimilation contains a flag indicating substantial or severe contamination by RFI, it is not able to capture small sources of just few Kelvin, which may be enough to wrongly interpret the signal as episodes of rainfall or higher

evapotranspiration than those in reality. Yet, the SEKF quality control is able to get rid of many of these small sources of RFI, as shown in Fig. 2c, but surely some contaminated observations still will be assimilated and will influence the accuracy of the analyses. A further study focusing on this aspect is recommended.

5   Conclusions

This paper has three main objectives: 1) demonstrate the feasibility of assimilating direct T_B in the ECMWF operational land surface data assimilation system, i.e., complementing the routine assimilation of screen level variables and ASCAT soil moisture retrievals, 2) investigate the added value of this new type of observation to provide more accurate soil moisture states, 3) evaluate the meteorological impact over relatively long-term periods.

The first objective has involved complex technical challenges as discussed above. Based on the data flow and results obtained in this paper, the feasibility of incorporating SMOS data in the soil moisture analysis has been demonstrated.

For the second objective, soil moisture analyses and forecasts were compared to in situ data from different networks in the US and Europe. The results of the evaluation exercise have shown that the best matching of analyses and forecasts to ground data was achieved when SMOS T_B were assimilated alone. The improvement is more pronounced for the top layer where the satellite signal carries direct information of soil moisture. With the setup of these experiments, the adjustment of the soil moisture background state was, on average, small over the period under investigation. This made the Open Loop experiment also obtain relatively good skill on soil moisture states. SMOS data tends to globally dry the soil of the ECMWF model. This is consistent with a wet biased model as documented in previous studies. Although the sign of the ASCAT increments for the top soil layer showed the opposite sign to SMOS T_B, they were quite small and therefore they still compared well to in situ observations. Larger absolute increments were obtained due to the assimilation of screen level variables, which is a consequence of having 2D gridded fields of 2 m temperature and 2 m relative humidity (generated by an OI scheme) available at each synoptic time. The adjustment of the soil states by screen variables has as main objective keeping air temperature and humidity errors at a minimum. The latter is very beneficial for atmospheric variables, as demonstrated by very good scores of meteorological variables such as air temperature and humidity, low-cloud cover or mean sea level pressure, when compared to an open loop. However, it was demonstrated that this was achieved at the expense of degrading the soil moisture state, although strictly speaking the relatively short evaluation period makes this degradation statistically non significant. Therefore, contrary to the theoretical idea that an improvement of the soil moisture state would be followed by an improvement of the lower atmospheric state, the model's reality is different and more complex. The previous statement would be true if the physical coupling processes between root-zone moisture and the near surface atmosphere were realistically simulated in the IFS model. On the contrary, they are related through a number of nonlinear equations and parameterizations, many of which use coefficients that have been tuned at local scale from field or regional-scale experiments. The application at global scale introduces errors which are reflected into poorer soil moisture analyses. The focus has not been on obtaining a realistic soil moisture state. The consequence is that if the only source of assimilated data is remote sensing data, then no significant improvement is seen in near-surface temperature or relative humidity. Hence our current system demands the use of screen level variables.

Our study has demonstrated the complexity of a system that was originally designed to use soil moisture as a tuning parameter to obtain the right upwelling fluxes. The family of ESA Earth explorers satellite missions addresses key scientific challenges identified by the science community and demonstrates

breakthrough technology in observing techniques. SMOS, has demonstrated its ability to bring unprecedented information on soil moisture. It has also been tremendously useful to understand the complexity of assimilating direct remote sensing data into a surface scheme coupled to the atmosphere, but also to point in the direction where future research should be directed, in particular where the interaction between land and atmosphere in the ECMWF forecast model can be improved.

Acknowledgements

References

[Albergel et al., 2012] Albergel, C., de Rosnay, P., Gruhier, C., Sabater, J. M., Hasenauer, S., Isaksen, L., Kerr, Y., and Wagner, W. (2012). Soil moisture analyses at ECMWF: Evaluation using global ground-based in situ observations. *J. Hydrometeor.*, 13:1442–1460. doi:10.1175/JHM-D-11-0107.1.

[Albergel et al., 2013] Albergel, C., Dorigo, W., Reichle, R., Balsamo, G., de Rosnay, P., Sabater, J. M., Isaksen, L., de Jeu, R., and Wagner, W. (2013). Skill and Global Trend Analyis of Soil Moisture from Reanalyses and Microwave Remote Sensing. *J. Hydrometeor.*, 14(4):1259–1277. doi:10.1175/JHM-D-12-0161.1.

[Albergel et al., 2009] Albergel, C., Rüdiger, C., Carrer, D., Calvet, J., Fritz, N., Naeimi, V., Bartalis, Z., and Hasenauer, S. (2009). An evaluation of ASCAT surface soil moisture products with in-situ observations in Southwestern France. *Hydrol. Earth Syst. Sci.*, 13:115–124.

[Balsamo et al., 2009] Balsamo, G., Viterbo, P., Beljaars, A., van den Hurk, B., Hirschi, M., Betts, A., and Scipal, K. (2009). A revised hydrology for the ECMWF model: Verification from field site to terrestrial water storage and impact in the integrated forecast system. *Journal of Hydrometeorology*, 10:623–643. doi: 10.1175/2008JHM1068.1.

[Bartalis et al., 2007] Bartalis, Z., Wagner, W., Naeimi, V., Hasenauer, S., Scipal, K., Bonekamp, H., Figa, J., and Anderson, C. (2007). Initial soil moisture retrievals from the METOP-A Advanced Scatterometer (ASCAT). *Geophys. Res. Lett.*, 34. L20401, doi:10.1029/2007GL031088.

[Beljaars et al., 1996] Beljaars, A. C. M., Viterbo, P., and Miller, M. (1996). The anomalous rainfall over the United States during July 1993: Sensitivity to land surface parameterization and soil moisture anomalies. *J. Hydrometeor.*, 124(3):362–383.

[Bell et al., 2013] Bell, J., Palecki, M., Baker, C., Collins, W., Lawrimore, J., Leeper, R., Kochendorfer, M. H. J., Meyers, T., Wilson, T., and Diamond, H. (2013). U.S. Climate Reference Network Soil Moisture and Temperature Observations. *J. Hydrometeor.*, 14(3):977–988.

[Boussetta et al., 2013] Boussetta, S., Balsamo, G., Beljaars, A., and Jarlan, J. (2013). Impact of a satellite-derived leaf area index monthly climatology in a global numerical weather prediction model. *International Journal of Remote Sensing*.

[Calvet et al., 2007] Calvet, J., Fritz, N., Froissard, F., Suquia, D., Petitpa, A., and Piguet, B. (2007). In situ soil moisture observations for the cal/val of smos: the smosmania network. In *2007 IEEE International Geoscience and Remote Sensing Symposium*, pages 1196–1199.

[Daganzo-Eusebio et al., 2013] Daganzo-Eusebio, E., Oliva, R., Kerr, Y. H., Nieto, S., Richaume, P., and Mecklenburg, S. M. (2013). SMOS Radiometer in the 14001427-MHz Passive Band: Impact of the RFI Environment and Approach to Its Mitigation and Cancellation. *TGARSs*, 51(10):4999–5007.

[de Lannoy and Reichle, 2016a] de Lannoy, G. and Reichle, R. (2016a). Assimilation of SMOS brightness temperatures or soil moisture retrievals into a land surface model. *HESSs*, 20:4895–4911.

[de Lannoy and Reichle, 2016b] de Lannoy, G. and Reichle, R. (2016b). Global Assimilation of Multi-angle and Multipolarization SMOS Brightness Temperature Observations into the GEOS-5 Catchment Land Surface Model for Soil Moisture Estimation. *JHs*, 17(2):669–691.

[de Rosnay et al., 2009] de Rosnay, P., Drusch, M., Boone, A., Balsamo, G., Decharme, B., Harris, P., Kerr, Y., Pellarin, T., Polcher, J., and Wigneron, J.-P. (2009). AMMA Land Surface Model Inter-comparison Experiment coupled to the Community Microwave Emission Model: ALMIP-MEM. *J. Geophys. Res.*, 114. D05108, doi:10.1029/2008JD010724.

[de Rosnay et al., 2013] de Rosnay, P., Drusch, M., Vasiljevic, D., Balsamo, G., Albergel, C., and Isaksen, L. (2013). A Simplified Extended Kalman Filter for the global operational soil moisture analysis at ECMWF. *Quart J. Roy. Meteor. Soc.*, 139(674):1199–1213. doi: 10.1002/qj.2023.

[de Rosnay et al., 2018] de Rosnay, P., Muñoz-Sabater, J., Albergel, C., Isaksen, L., .Drusch, M., and Wigneron, J. (2018). SMOS brightness temperature forward modelling, bias correction and long term monitoring at ECMWF. Submitted to Remote Sensing.

[Dorigo et al., 2011] Dorigo, W., Wagner, W., Hohensinn, R., Hahn, S., Paulik, C., Xaver, A., Gruber, A., Drusch, M., Mecklenburg, S., van Oevelen, P., Robock, A., and Jackson, T. (2011). The international soil moisture network: a data hosting facility for global in situ soil moisture measurements. *Hydrol. Earth Syst. Sci.*, 15:1675–1698.

[Douville et al., 2000] Douville, H., Viterbo, P., Mahfouf, J., and Beljaars, A. (2000). Evaluation of optimal interpolation and nudging techniques for soil moisture analysis using FIFE data. *Mon. Wea. Rev.*, 128:1733–1756.

[Draper et al., 2012] Draper, C., Reichle, R., de Lannoy, G., and Liu, Q. (2012). Assimilation of passive and active microwave soil moisture retrievals. *Geophys. Res. Lett.*, 39. L04401, doi:10.1029/2011GL050655.

[Drusch et al., 2009a] Drusch, M., Holmes, T., de Rosnay, P., and Balsamo, G. (2009a). Comparing ERA-40 based L-band brightness temperatures with Skylab observations: A calibration / validation study using the Community Microwave Emission Model. *J. Hydrometeor.*, 10:213–226. doi: 10.1175/2008JHM964.1.

[Drusch et al., 2009b] Drusch, M., Scipal, K., de Rosnay, P., Balsamo, G., Andersson, E., Bougeault, P., and Viterbo, P. (2009b). Towards a Kalman filter based soil moisture analysis system for the operational ECMWF Integrated Forecast System. *Geophys. Res. Lett.*, 36. doi:10.1029/2009GL037716, 2009.

[Drusch and Viterbo, 2007] Drusch, M. and Viterbo, P. (2007). Assimilation of screen-level variables in ECMWF's Integrated Forecast System: A study on the impact of the forecast quality and analyzed soil moisture. *Mon. Wea. Rev.*, 135(2):300–314. doi - 10.1175/MWR3309.1.

[Drusch et al., 2005] Drusch, M., Wood, E., and Gao, H. (2005). Observation operators for the direct assimilation of trmm microwave imager retrieved soil moisture. *Geophys. Res. Lett.*, 32(15). doi:10.1029/2005GL023623.

[Drusch et al., 2001] Drusch, M., Wood, E., and Jackson, T. (2001). Vegetative and atmospheric corrections for the soil moisture retrieval from passive microwave remote sensing data: Results from the southern great plains hydrology experiment 1997. *J. Hydrometeor.*, 2(2):181–192.

[Gao et al., 2006] Gao, H., Wood, E., Jackson, T., Drusch, M., and Bindlish, R. (2006). Using TRMM/TMI to Retrieve Surface Soil Moisture over the Southern United States from 1998 to 2002. *J. Hydrometeor.*, 7(doi: 10.1175/JHM473.1):23–38.

[Gao et al., 2017] Gao, Q., Zribi, M., Escorihuela, M., and Baghdadi, N. (2017). Synergetic Use of Sentinel-1 and Sentinel-2 Data for Soil Moisture Mapping at 100 m Resolution. *Sensors*, 17(9, doi: 10.3390/s17091966).

[Geer, 2016] Geer, A. (2016). Significance of changes in medium-range forecast scores. *Tellus A: Dynamic Meteorology and Oceanography*, 68(1):30229.

[Haiden et al., 2018] Haiden, T., Sandu, I., Balsamo, G., Arduini, G., and Beljaars, A. (2018). Addressing biases in near-surface forecasts. Technical Report 157, European Centre for Medium-Range Weather Forecasts, Reading, United Kingdom.

[IFS documentation, 2017] IFS documentation (2017). *IFS Documentation Cycle 43R3; Part II: Data Assimilation*. ECMWF, Shinfield Road, RG2 9AX, Reading, UK. photocopy.

[Kerr et al., 2016] Kerr, Y., Al-Yaari, A., Rodriguez-Fernandez, N., Parrens, M., Molero, B., Leroux, D., Bircher, S., Mahmood, A., Mialon, A., Richaume, P., Delwart, S., Bitar, A. A., Pellarin, T., Bindlish, R., Jackson, T., Rüdiger, C., Waldteuf, P., Mecklenburg, S., and Wigneron, J.-P. (2016). Overview of SMOS performance in terms of global soil moisture monitoring after six years in operation. *Remote Sens. of Environ.*, 180:40–63.

[Kerr et al., 2012] Kerr, Y., Font, J., Martin-Neira, M., and Mecklenburg, S. (2012). Introduction to the special issue on the ESA's Soil Moisture and Ocean Salinity Mission (SMOS) instrument performance and first results. *IEEE Trans. Geosc. Remote Sens.*, 50:1351–1353.

[Kerr et al., 2010] Kerr, Y., Waldteufel, P., Wigneron, J.-P., Delwart, S., Cabot, F., Boutin, J., Escorihuela, M., Font, J., Reul, N., Gruhier, C., Juglea, S., Drinkwater, M., Hahne, A., Martin-Neira, M., and Mecklenburg, S. (2010). The SMOS mission: New tool for monitoring key elements of the Global Water Cycle. *Proc. IEEE*, 98(5):666–687.

[Koster et al., 2011] Koster, R., abd T.J. Yamada, P. M., Balsamo, G., Berg, A., Boisserie, M., Dirmeyer, P., Doblas-Reyes, F., Drewitt, G., Gordon, C., Guo, Z., Jeong, J., Lee, W., Li, Z., Luo, L., Malyshev, S., Merryfield, W., Seneviratne, S., Stanelle, T., den Hurk, B. V., Vitart, F., and Wood, E. (2011). The second phase of the global land-atmosphere coupling experiment: soil moisture contribution to subseasonal forecast skill. *J. Hydrometeor.*, 12:805–822.

[Koster et al., 2010] Koster, R., Mahanama, S., Yamada, T., Balsamo, G., Dirmeyer, A. B. M. B. P., Doblas-Reyes, F., Drewitt, G., Gordon, C., Guo, Z., Jeong, J., Lawrence, D., Lee, W., Li, Z., Luo, L., Malyshev, S., Merryfield, W., Seneviratne, S., Stanelle, T., van den Hurk, B., Vitart, F., and Wood, E. F. (2010). Contribution of land surface initialization to subseasonal forecast skill: First results from a multi-model experiment. *Geophys. Res. Lett.*, 37(2). L02402, doi:10.1029/2009GL041677.

[Li et al., 2010] Li, L., Gaiser, P., Gao, B., Bevilacqua, R., Jackson, T., Njoku, E., Rüdiger, C., Calvet, J., and Bindlish, R. (2010). Windsat global soil moisture retrieval and validation. *IEEE Trans. Geosc. Remote Sens.*, 48(5):2224–2241.

[Lievens et al., 2016] Lievens, H., Lannoy, G. D., Bitar, A. A., Drusch, M., Dumedah, G., Franssen, H.-J. H., Kerr, Y., Tomer, S., Martens, B., Merlin, O., Pan, M., Roundy, J., Vereecken, H., Walker, J., Wood, E., Verhoest, N., and Pauwels, V. (2016). Assimilation of SMOS soil moisture and brightness temperature products into a land surface model. *Remote Sens. of Environ.*, 180:292–304.

[Lievens et al., 2015] Lievens, H., Tomer, S., Bitar, A. A., Lannoy, G. D., Drusch, M., Dumedah, G., Franssen, H., Kerr, Y., Martens, B., Pan, M., and Roundy, J. (2015). SMOS soil moisture assimilation for improved hydrologic simulation in the Murray Darling Basin, Australia. *RSEs*, 168:146–162.

[Loveland et al., 2000] Loveland, T., Reed, B., Brown, J., Ohlen, D., Zhu, Z., Youing, L., and Merchant, J. (2000). Development of a global land cover characteristics database and IGB6 DISCover from the 1 km AVHRR data. *International Journal of Remote Sensing*, 21:1303–1330.

[Mahfouf, 1991] Mahfouf, J.-F. (1991). Analysis of soil moisture from near-surface parameters: a feasibility study. *Journal of Applied Meteorology*, 30:1534–1547.

[Mahfouf et al., 2000] Mahfouf, J.-F., Viterbo, P., Douville, H., Beljaars, A., and Saarinen, S. (2000). A revised land surface analysis scheme in the integrated forecasting system. Technical Report 88, European Centre for Medium-Range Weather Forecasts, Reading, United Kingdom.

[Martinez-Fernandez and Ceballos, 2003] Martinez-Fernandez, J. and Ceballos, A. (2003). Temporal Stability of Soil Moisture in a Large-Field Experiment in Spain. *Nature*, 67(SSSAJs):1647–1656.

[Materia et al., 2014] Materia, S., Borrelli, A., Bellucci, A., Alessandri, A., Pietro, P. D., Athanasiadis, P., Navarra, A., and Gualdi, S. (2014). Impact of atmosphere and land surface initial conditions on seasonal forecasts of global surface temperature. *J. Climate*, 27:92539271.

[Mecklenburg et al., 2016] Mecklenburg, S., Drusch, M., Kaleschke, L., Rodriguez-Fernandez, N., Reul, N., Kerr, Y., Font, J., Martin-Neira, M., Oliva, R., Daganzo-Eusebio, E., Grant, J., Sabia, R., Macelloni, G., Rautiainen, K., Fauste, J., de Rosnay, P., Muñoz-Sabater, J., Verhoest, N., Lievens, H., Delwart, S., Crapolicchio, R., de la Fuente, A., and Kornber, M. (2016). Esa's soil moisture and ocean salinity mission: From science to operational applications. *Remote Sens. of Environ.*, 180:3–18.

[Muñoz-Sabater, 2015] Muñoz-Sabater, J. (2015). Incorporation of passive microwave brightness temperatures in the ecmwf soil moisture analysis. *Remote Sensing*, 7(5):5758–5784.

[Muñoz-Sabater et al., 2014a] Muñoz-Sabater, J., Dahoui, M., de Rosnay, P., and Isaksen, L. (2014a). SMOS Monitoring Report; Number IV: Jan. 2013 - Dec. 2013. Technical report, European Centre for Medium-Range Weather Forecasts, Reading, United Kingdom.

[Muñoz-Sabater et al., 2018] Muñoz-Sabater, J., de Rosnay, P., Albergel, C., and Isaksen, L. (2018). Sensitivity of soil moisture analyses to contrasting background and observation error scenarios. *Water*, 10(7).

[Muñoz-Sabater et al., 2011] Muñoz-Sabater, J., de Rosnay, P., and Balsamo, G. (2011). Sensitivity of L-band NWP forward modelling to soil roughness. *Int. J. Remote Sens.*, 32(19):5607–5620. iFirst 2011., doi: 10.1080/01431161.2010.507260.

[Muñoz-Sabater et al., 2014b] Muñoz-Sabater, J., de Rosnay, P., Jiménez, C., and Isaksen, L. (2014b). SMOS brightness temperatures angular noise: characterization, filtering and validation. *IEEE Transactions on Geoscience and Remote Sensing*, 52(9):5827–5839.

[Muñoz-Sabater et al., 2012] Muñoz-Sabater, J., Fouilloux, A., and de Rosnay, P. (2012). Technical implementation of SMOS data in the ECMWF Integrated Forecasting System. *Geosc. Remote Sens. Letters*, 9(2):252–256.

[Naeimi et al., 2009] Naeimi, V., Bartalis, Z., and Wagner, W. (2009). ASCAT Soil Moisture: An Assessment of the Data Quality and Consistency with the ERS Scatterometer Heritage. *JHs*, 10(2):555–563.

[Oliva et al., 2016] Oliva, R., Daganzo, E., Richaume, P., Kerr, Y., Cabot, F., Soldo, Y., Anterrieu, E., Reul, N., Gutierrez, A., Barbosa, J., and Lopes, G. (2016). Status of Radio Frequency Interference (RFI) in the 1400-1427 MHz passive band based on six years of SMOS mission. *Remote Sens. of Environ.*, 180:64–75.

[Pellarin et al., 2003] Pellarin, T., Wigneron, J.-P., Calvet, J.-C., and Waldteufel, P. (2003). Global soil moisture retrieval from a synthetic l-band brightness temperature data set. *Journal of Geophysical Research*, 108(4364, doi:10.1029/2002JD003086).

[Prodhomme et al., 2016] Prodhomme, C., Doblas-Reyes, F., Bellprat, O., and Dutra, E. (2016). Impact of land-surface initialization on sub-seasonal to seasonal forecasts over europe. *Clim. Dynamics*, 47(doi: 10.1007/s00382-015-2879-4):919–935.

[Reichle and Koster, 2004] Reichle, R. and Koster, R. (2004). Bias reduction in short records of satellite soil moisture. *Geophys. Res. Lett.*, 31(L19510).

[Reichle and Koster, 2005] Reichle, R. and Koster, R. (2005). Global assimilation of satellite surface soil moisture retrievals into the NASA Catchment land surface model. *Geophys. Res. Lett.*, 32(2). L02404, doi:10.1029/2004GL021700.

[Schaefer et al., 2007] Schaefer, G., Cosh, M., and Jackson, T. (2007). The USDA Natural Resources Conservation Service Soil Climate Analysis Network (SCAN). *J. Atmos. Oceanic Technol.*, 24:2073–2077.

[Scipal et al., 2008] Scipal, K., Drusch, M., and Wagner, W. (2008). Assimilation of an ERS scatterometer-derived soil moisture index in the ECMWF numerical weather prediction system. *Adv. Water Resour.*, 31:1101–1112.

[Scipal et al., 2005] Scipal, K., Naeimi, V., and Hasenauer, S. (2005). Definition of Quality Flags. In ASCAT Soil Moisture Report Series. Technical report, Institute of Photogrammetry and Remote Sensing. Vienna University of Technology. Report 7, 25 pp.

[Seuffert et al., 2004] Seuffert, G., Wilker, H., Viterbo, P., Drusch, M., and Mahfouf, J. F. (2004). The usage of screen-level parameters and microwave brightness temperature for soil moisture analysis. *Journal of Hydrometeorology*, 5(3):516–531.

[Van-Den-Hurk et al., 2008] Van-Den-Hurk, B., Ettema, J., and Viterbo, P. (2008). Analysis of soil moisture changes in Europe during a single growing season in a new ECMWF soil moisture assimilation system. *J. Hydrometeor.*, 9:116–131.

[Verhoest et al., 2015] Verhoest, N. E. C., van den Berg, M. J., Martens, B., Lievens, H., Wood, E. F., Pan, M., Kerr, Y. H., Bitar, A. A., Tomer, S. K., Drusch, M., Vernieuwe, H., Baets, B. D., Walker, J. P., Dumedah, G., and Pauwels, V. R. N. (2015). Copula-Based Downscaling of Coarse-Scale Soil Moisture Observations With Implicit Bias Correction. *TGARSs*, 53(6):3507–3521. doi:10.1109/TGRS.2014.2378913.

[Viterbo, 1996] Viterbo, P. (1996). *The representation of surface processes in general circulation models*. PhD thesis, University of Lisbon.

[Viterbo and Beljaars, 1995] Viterbo, P. and Beljaars, A. C. M. (1995). An Improved Land Surface Parameterization Scheme in the ECMWF Model and Its Validation. *JCS*, 8(11):2716–2748. doi:10.1175/1520-0442(1995)008¡2716:AILSPS¿2.0.CO;2.

[Wagner et al., 2007] Wagner, W., Bloschl, G., Pampaloni, P., Calvet, J., Bizzarri, B., Wigneron, J., and Kerr, Y. (2007). Operational readiness of microwave remote sensing of soil moisture for hydrologic applications. *Hydrol. Res.*, 38(1). doi: 10.2166/nh.2007.029.

[Wagner et al., 2013] Wagner, W., Hahn, S., Kidd, R., Melzer, T., Bartalis, Z., Hasenauer, S., Figa-Saldaña, J., de Rosnay, P., Jann, A., Scheiner, S., Komma, J., Kubu, G., Brugger, K., c. Aubrecht, Züger, J., Gangkofner, U., Kienberger, S., Brocca, L., Wang, Y., Blöschl, G., Eitzinger, J., Steinnocher, K., Zeil, P., and Rubel, F. (2013). The ASCAT Soil Moisture Product: A review of its specifications, Validation Results, and Emerging Applications. *Meteorologische Zeitschrift*, 22(1):5–33. doi: 10.1127/0941-2948/2013/0399.

[Wagner et al., 1999] Wagner, W., Lemoine, G., and Rott, H. (1999). A Method for Estimating Soil Moisture from ERS Scatterometer and Soil Data. *Remote Sens. of Environ.*, 70(2):191–207. doi:10.1016/S0034-4257(99)00036-X.

[Wang and Schmugge, 1980] Wang, J. R. and Schmugge, T. (1980). An empirical model for the complex dielectric permittivity of soils as a function of water content. *IEEE Transactions on Geoscience and Remote Sensing*, 18:288–295.

[Weisheimer et al., 2011] Weisheimer, A., Doblas-Reyes, P., Jung, T., and Palmer, T. (2011). On the predictability of the extreme summer 2003 over Europe. *Geophys. Res. Lett.*, 38.

[Wen et al., 2005] Wen, J., Jackson, T., Bindlish, R., Hsu, A., and Su, Z. B. (2005). Retrieval of soil moisture and vegetation water content using ssm/i data over a corn and soybean region. *J. Hydrometeor.*, 6(6):854–863.

[Wigneron et al., 2007] Wigneron, J.-P., Kerr, Y., Waldteufel, P., Saleh, K., Escorihuela, M.-J., Richaume, P., Ferrazzoli, P., de Rosnay, P., Gurneye, R., Calvet, J.-C., Grant, J., Guglielmetti, M., Hornbuckle, B., Mtzler, C., Pellarin, T., and Schwank, M. (2007). L-band microwave emission of the biosphere (L-MEB) model: Description and calibration against experimental data sets over crop fields. *Remote Sensing of Environment*, 107(4):639–655.

[Wigneron et al., 2001] Wigneron, J. P., Laguerre, L., and Kerr, Y. (2001). A simple parameterization of the L-band microwave emission from rough agricultural soils. *IEEE Transactions on Geoscience and Remote Sensing*, 39:1697–1707.

6 Appendix

The figures below are complementary of those shown in section 3.6, and show atmospheric forecast scores for air temperature, low cloud cover, sea level pressure and geopotential height.
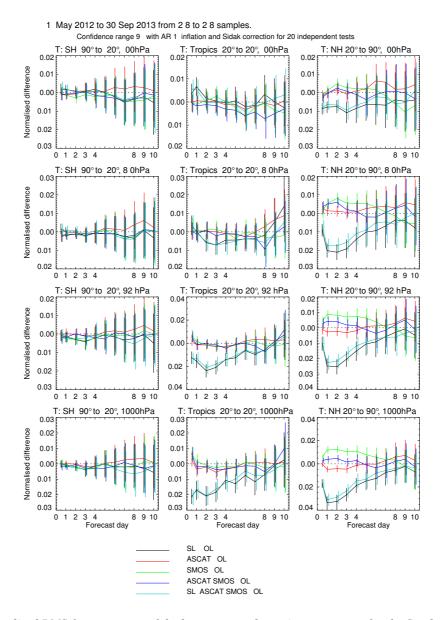

*Figure 15: Normalized RMS forecast error of the lower troposphere air temperature for the Southern Hemisphere extra tropics region (left column), Tropics (middle column) and Northern Hemisphere extra-tropics (right column), and for the 700 hPa (top row), 850 hPa (second row), 925 hPa (third row) and 1000 hPa (bottom row) pressure levels. The black curve is for the **SLV** experiment, red curve for **ASCAT**, green curve for **SMOS**, dard blue for **SMAS** and light blue for **SLVSMAS**. All of them are compared (and normalized) to the **OL** experiment. The forecast period is May-Sept 2012 and 2013, combined.*
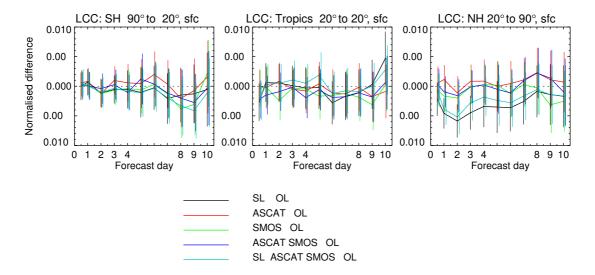
Figure 16: Normalized RMS forecast error of the tropospheric averaged low cloud cover for the South Hemisphere extra tropics region (left column), Tropics (middle column) and North-Hemisphere extra-tropics (right column). The black curve is for the **SLV** experiment, red curve for **ASCAT**, green curve for **SMOS**, dark blue for **SMAS** and light blue for **SLVSMAS**. All of them are compared (and normalized) to the **OL** experiment. The forecast period is May-Sept 2012 and 2013, combined.
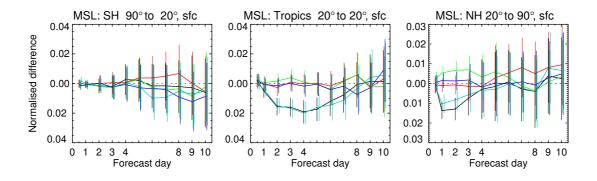
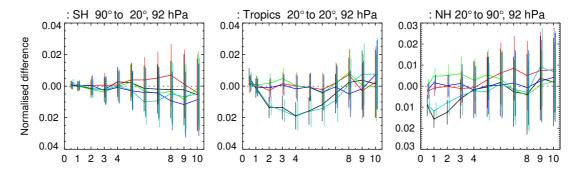

Figure 17: As Fig. 16 but for the mean sea level pressure.

Figure 18: As Fig. 16 but for the geopotential height at 925 hPa.